

# Author response for "Quantifying the potential future contribution to global mean sea level from the Filchner-Ronne basin, Antarctica"

Emily A. Hill<sup>1,2</sup>, Sebastian H. R. Rosier<sup>2</sup>, G. Hilmar Gudmundsson<sup>2</sup>, and Matthew Collins<sup>1</sup>

<sup>1</sup>College of Engineering, Mathematics and Physical Sciences, University of Exeter, Exeter, United Kingdom

<sup>2</sup>Department of Geography and Environmental Sciences, University of Northumbria, Newcastle-upon-Tyne, United Kingdom

We extend our thanks to Anonymous Referee 1 and Nicolas Jourdain for their positive feedback on our manuscript and constructive comments that will greatly help to improve the manuscript. We have addressed all of the comments and made the necessary changes to the manuscript. Below are our responses, where referee comments are in black, and our replies are in blue. A tracked-changes version of the manuscript is also included at the end of this document.

Best wishes,

Emily Hill and co-authors

## Response to comments from Anonymous Referee 1

This manuscript describes a set of experiments using the ice flow model  $\dot{U}_a$ , aimed at characterizing the spread of possible future sea level contribution from the Filchner-Ronne (FR) drainage basin. The authors create a set of ensemble simulations, under various RPC emission scenarios, that extend to the year 2300, and use these simulations to build a surrogate model. To create their ensemble, the authors sample parameters related to ocean forcing, atmospheric forcing, and ice dynamics within bounds they derive from literature, climate model ensembles of future projections, and Bayesian analysis (for the ocean forcing parameters). The authors illustrate that the surrogate model exhibits skill in predicting the sea level contribution projected by  $\dot{U}_a$  in the FR region by year 2300, and they then use the surrogate to create a million-sample distribution to represent the possible spread of sea level contribution from FR within the same period. Surrogates are also created to derive estimates of sea-level contribution at years 2100 and 2200, for analysis of projected sea level contribution through time. Results suggest that the FR region is not likely to contribute positively to sea level contribution in the future, largely due to the modeled increase in accumulation over time in response to warming atmospheric conditions. However, significant contribution to sea level from this region is found to be possible (more than >30cm by year 2300), though this outcome is not probable. The author's analysis also allowed them to isolate contribution to uncertainty from the various model parameters sampled, and they

find that atmospheric and ocean forcing account for the majority of the sea-level projection uncertainty, in agreement with past studies. The authors specifically highlight these model boundary conditions as the most important to improve models of in order to increase confidence in ice sheet model projections of sea level contribution.

Here, the authors present a novel approach to the challenge of quantifying uncertainties in ice sheet model projections. Running the number of model simulations required for robust assessment of uncertainties is, in many cases, not computationally feasible, so the design of an adequate surrogate model for this purpose is highly advantageous. Overall, I find that the authors thoroughly describe their methods, experiments, reasoning, and caveats. The discussion, in particular, highlights the care that must be taken when considering results from a single ice sheet model where specific assumptions are necessary to produce realistic model ensembles. The manuscript is well-written and the figures are highly illustrative of the methods and results. The workflow diagram (Fig. 2), is especially helpful in describing the investigation's strategy. In addition, the results are thorough and well-organized, therefore I find this manuscript highly appropriate for publication in the Cryosphere, with revisions and some supporting analysis.

We are very grateful to Referee 1 for taking the time to review our manuscript and for their positive feedback.

I have a number of questions and comments for the authors, as listed below, for author response and discussion.

General comments:

Discussion section – The discussion is quite thorough, and you cover many important points and caveats. However, I think it would be improved if you also expand upon some interesting topics that are brought up in the results section, specifically pertaining to the advantages and disadvantages of using a surrogate model for this analysis. For example, in the results section, you note an example of an advantage of using the surrogate, can you expand upon this in the discussion to talk about what you learned in that exercise with respect to the importance of including extremes in your training set? Could you also expand upon what might be the disadvantages or pitfalls that others using your methods could encounter? (For example, is there a danger of not capturing threshold behavior or runaway retreat, as you observe in some of your extreme forcing simulations?) Is it possible that runaway retreat is more likely than your training set suggests, or do you think that your sampling space and final pdf capture the spread of possible scenarios accurately?

Thank you for your suggestion to include more details on the advantages and disadvantages of using the surrogate model. We have partly responded to this in the next point, and made changes to the Results section to reflect how our training ensemble and surrogate model are different/similar in terms of the projections. We have also added a couple of extra sentences to the start of the final paragraph of the Discussion to tie this through and make it clear that our surrogate model has been a powerful tool for gaining additional insight into the future of this region, beyond what we would have gained from our (already large)

ensemble alone. We had already tried to make an effort to discuss some of the disadvantages of our method in relation to capturing the regime shift seen in the Hellmer et al. 2012 paper in the 6th paragraph of the Discussion. However, this was mainly due to the choice of melt parameterisation and slow increase in melt rates rather than a sudden flush of warm water that could be achieved with an ocean circulation model. We agree that this could partly be due to parameter space we have chosen for the ocean forcing parameters. One of your later comments also touches upon this, that our Bayesian inferred melt rates may be lower (but potentially more realistic), which has prevented us from sampling high melt distributions akin to a tipping point in the Weddell Sea. We've added a sentence to the 6th paragraph of the Discussion to reflect this. It is difficult to make more conclusive statements about whether runaway retreat is more likely than our training set suggests. The approach we have used does of course mean that our final pdfs are somewhat governed by the uncertainties/prior probability distributions we use for our input parameters. While we have tried to make our prior pdfs as informed as possible, which is challenging for some parameters, and in those cases we have had no choice but to assume equal probability and sample from uniform distributions. This would then effect the likelihood of extreme events and in that respect could be considered a limitation of our method. However, we have made it clear in the Discussion that our sampling and surrogate model has been able to capture a similar magnitude of basal melting to Hellmer et al. 2012, which reflects high-melt scenarios. It is of course possible that the likelihood of these extreme events could be more or less with a change in the priors, as mentioned above. Future improved constraints on our input parameters would help to provide more informed projections.

In addition, how important was it to use a surrogate to capture the full sample space? That is, do your final pdf's reveal a different pdf than your ensembles suggest? Perhaps you can show some training run (ensemble) pdf's vs. the surrogate sampling pdf's in the appendix to illustrate this point.

The final pdf's of our surrogate model versus those generated by the training ensemble are shown in Figure 6, where the tail of the surrogate model pdf extends beyond the spread of the ensemble in 2300. We appreciate that this is not easy to see for scenarios other than RCP 8.5 but are not sure we need an additional figure. The likely range (5-95%) of our results to not change dramatically between the training ensemble and the surrogate model. Despite the similarities between our ensemble/surrogate model in the likely range, we have still gained valuable additional insights by using a surrogate model. While the high magnitude contributions to sea level rise in RCP 8.5 are unlikely, they still highlight their potential within our parameter space, and what this means for ice loss, and runaway grounding line retreat. This means that our surrogate model highlighted the possibility of more extreme sea level rise scenarios that were not exposed by the original sample. We have added a further sentence to the end of Section 4.1 of the Results that makes this point point clear.

Specific questions and suggestions:

Line 1: This opening sentence is a bit awkward to read. Maybe adding “The future . . .” => “change”, “behavior”, or “evolution” or a similar phrase would make your point clearer.

This sentence has been revised in the manuscript to read better.

Line 34: . . . as the “combined area” of the two major drainage basins. . . (or something similar)

This has been added in the manuscript

Line 55: I understand the point you are trying to make in this sentence, but it reads awkwardly. Please try rephrasing.

Agreed. This sentence has been rephrased in the manuscript

Line 159: Could you add a thin or dashed line to Fig 1 or its small inset that shows where the divide between the two basins sits?

A dashed line and labels for the two drainage basins has been added to the inset of Figure 1, and the caption updated to reflect these changes.

Line 162: Perhaps in the supplement, an illustration of what your mesh looks like, perhaps in some key locations, would be very helpful.

A Figure of the model mesh has been added to the supplement, which includes an inset that shows the mesh around the Rutford Ice Stream in more detail. A reference to this figure has been added in the main text.

Line 170: Could you please specify the settings for your initial mesh adaption, for instance: What is your minimum mesh for the adaption? Is it still 900m? Is there a maximum mesh size near the grounding line? How close to the grounding line is the adaption imposed (i.e. is there a set buffer length)?

Additional details on the element sizes have been added to the text, including that elements within a 10 km distance of the grounding line are 3 km and 900 m within a 1.5 km's of the grounding line.

Line 171: What is the minimum thickness value that is imposed?

30 m. This has been added to the text.

Line 235: You discuss only changes to surface accumulation through time. Do your simulations have a representation of surface melt as well (i.e., a PDD scheme or something similar)? Please specify this in the text.

We have now added a sentence to the text in Section 3.3 that makes it clear that we are not representing surface melt using a PDD scheme for these regional simulations (see response to Referee 2 on a similar point). We have also added in some

justification, as the paper suggested by Referee 2 (Kittel et al., 2021) does not suggest that this region will experience negative surface mass balance, even under RCP 8.5 forcing.

Line 315: The term “point” is used a number of times in the text to refer to a location in your sampling space. This terminology is easy to confuse with a point in map space. Is it possible to use a more specific term, like “sample point” or something similar throughout the manuscript to distinguish between sampling space and actual 2d map space?

We have been through the manuscript and added sample point to make it clearer throughout that this is a point from a parameter space.

Line 322: Please quantify the model drift (or spread of model drift for all of your control runs) here.

We have now added in the range of model drift in mm of  $\Delta$ GMSL for the control runs

Line 328: Throughout the manuscript, you refer to this set of simulations as your “ensemble”. It would be helpful for the reader if you explicitly call out here that these are the runs that you will hereafter call the “ensemble” (or create a name for this set of runs that you can refer to later in the manuscript).

We have added `which we hereafter refer to as our "training ensemble", where it is first mentioned in the manuscript (the caption to Figure 2) and have changed it throughout the manuscript to make it clear which ensemble we are referring to.

Line 339: Please add a quantitative statement with respect to the surrogate model being “close” to the ice flow model response. We have now calculated the root mean square error between our modeled responses (from our validation sample) and the predictions from the surrogate model using the same validation X sample. Some lines have been added to the text, and RMSE for each surrogate model included on Supplementary Figure S2

Line 345: What type of algorithm is used for the sampling of these 1 million simulations? Is it Latin hypercube as in the other ensemble sampling?

Yes this was done using Latin hypercube sampling, and that has been added to the text.

Figure 5: Please note the year at which the sea GMSL represents in the plot or caption (i.e. 2300).

The caption already includes "by the year 2300"

Line 440: Please note in the text the simulations used for this analysis (i.e., the ensemble)

This has been added.

Line 530: While Ritz et al., 2015 do not change surface mass balance through time, Schlegel et al., 2018 apply a step function on accumulation, so there is still a possibility for suppression due to accumulation. The difference is more likely due to your treatment of ocean forcing (e.g., PICO with Bayesian exploration extreme melt rates, which may be lower but considered more realistic, especially with consideration to the possible time lag between atmosphere and ocean warming), as well as your application of no melt on partially floating elements, adaptive grounding line mesh, and even the repetition of inversion procedures for each model simulation.

This is a good point that there is a distinction between these two studies that we hadn't made clear in the text. We've separated the two, and brought the Schlegel reference and some additional explanation into the previous sentence. We have made reference to our Bayesian inferred melt rates in a following paragraph of the Discussion when we compare our results to those of Hellmer et al. 2012.

Line 535: Your results show a strong dependence on accumulation, and the discussion below gives an inclusive overview of the challenges in forcing accumulation on ice sheet models in general. Could you offer a quantitative comparison between the spread (pdf) of the change (anomaly) in precipitation that your sampling imposes on your simulations, and that that is predicted by CMIP5 models? For example, you present the spread in the ocean forcing time delay parameter from LARMIP-2, could you show similarly, maybe in the supplement, a similar pdf for your regional accumulation from various CMIP GCM's and then compare that against a pdf that represents accumulation sampling from the surrogate (or even just the ensemble?). I am curious to see this comparison, since while you sample  $p$  in a normal way (Fig. 3), this parameter is exponentially related to accumulation. Is it possible that this choice skews your sampling to higher sensitivity to temperature change? Is the imposed sampling of total increased accumulation realistic as compared to what GCM's are predicting? If not, this should be mentioned as a caveat in your discussion, because it has implications for the shape of your final GMSL pdfs (Fig. 5), and total probabilities.

This is a really interesting and relevant point. It is still an open question in the field as to whether parameterisations of accumulation change with warming used in ice sheet models are able to accurately replicate accumulation predictions in CMIP GCMs. It would almost be a separate study in itself to validate these, including selecting appropriate CMIP5 models to use, and extracting this information regionally for the FR basin. It would make for interesting future work, but is perhaps beyond the scope of this study. In the case of the LARMIP-2 time delay parameter, we were directly using this information as a prior to our Bayesian inference of melt rates. Of course if we were to tune the input distribution of our  $p$  parameter, based on it's ability to produce accumulation rates similar to GCMs then it would be appropriate to use the output of CMIP models as a target to constrain the distribution of  $p$ . However, doing this would also need some careful consideration as CMIP models themselves show large temporal and spatial variability in their predictions of precipitation, and some of them may not accurately replicate current precipitation changes. The values for  $p$  we use are taken from studies that have performed such an analysis and selected CMIP5 models that are able to replicate observations to derive the value of  $p$  (e.g. Palerme et al., 2017 - Climate Dynamics). The work of Rodehacke et al. 2019 also showed some of the challenges and stark contrasts between projections of sea level rise using either CMIP5 results directly, or a precipitation scaling, and perhaps suggests that using such scalings is a better option

than CMIP results, due to the uncertainties in CMIP data themselves. Using the spatially variable scaling they propose, would be an improvement to our approach in future. We can agree that sampling from a uniform distribution may have skewed the distribution of accumulation and had an impact on our on projections of  $\Delta\text{GMSL}$ . In the absence of additional information on the distribution of  $p$  (that indeed in the future could be constrained by observations/CMIP results), it is difficult to know what other distribution we could have used. Our approach here was really to say "this is the state of current parameterisations and knowledge of uncertainties in some of the parameters that are used and what happens when we propagate these uncertainties through our model" and not to validate the results to other model results. But we can agree that this is indeed a caveat to our results, and we have added a couple of sentences to the Discussion to reflect this.

Line 764: Could you quantify at what probability does the Reese et al., 2018a value sit in your distribution? Can you comment on the possible implications of your values sitting much lower in magnitude than suggested by this previous study? In Fig. S2 it appears that once the  $\gamma_T^*$  value approaches  $2 \times 10^{-5}$ , that the delta GMSL contribution starts to become highly negative. Can you discuss why that is and how it influences your resulting pdf from Fig. B1?

We have gone back and calculated the percentile in our distribution that the Reese et al., 2018 value sits, and it is indeed at the very extreme of our distribution at the approx. 99th percentile. It is not too surprising that we found a lower value, given that their goal was to calibrate an appropriate value for both Pine Island and Filchner-Ronne. It is a good point that the results of Figure S2 suggest that the GMSL contribution becomes highly negative in this region. I think it's important to note that the pdf in Figure B1 is only used as an input to our main uncertainty analysis, and is therefore not affected by the GMSL projections or main ensemble of simulations. However, it does of course affect the uncertainty range of our priors, and subsequent sampling to generate our training ensemble, and additionally the 1,000,000 point sample that was used to get our projections from the surrogate models. It is probably the case that because there were few training samples beyond  $2 \times 10^{-5}$ , that the surrogate model ultimately struggles to replicate the individual response to this parameter alone for these high values.

Line 766: basal mass balance?

Changed.

Figure S1: Please specify the simulation year of GMSL presented.

"By the year 2300" has been added to the figure caption

Figure S2: The results presented here are a bit puzzling. Are they, as other results, represented as difference from the control simulation? If so, if I am understanding your methods correctly, then I would expect all graphs to cross a value of zero  $\Delta\text{GMSL}$ , when the value of the sampled parameter is equal to the value of the control run. Could you speak to this, specifically why most of the graphs show a negative contribution to sea level for all of the sampled values?

This is a good point, and it is indeed correct that if the only difference between our control run and perturbed RCP runs was

the change in each parameter value, then they would indeed cancel out and cross zero. However, our control runs also do not contain time dependent forcing, whereas our perturbed runs are applying a temperature change that varies through time, which is why this is not the case. We already state that the control run has constant temperature forcing in Section 3.5, so do not feel that any further changes are needed to the text.

Figure S4: Please check the lettered labels on the right-hand column plots.

Lettered labels have been corrected

## Response to comments from Nicolas Jourdain

One of the two nominated referees had to cancel his/her participation for personal reasons. I nonetheless received a positive preliminary feedback on this work. To save time in the review process, I have therefore decided to write a review myself.

Thanks to Nicolas for stepping in to provide a second review of the paper at the last minute, we appreciate the additional feedback provided.

The paper reads well and the methods are robust and clearly described. The results are important for the ice-sheet and sea-level communities, and I only have a few minor comments that will hopefully improve the paper:

Thank you for the positive feedback on our manuscript and for your suggested improvements. As before, we respond to the comments below in blue text.

L. 136: effect -> effects

Changed

L. 165: “with a percentage deviation of only 3%” -> specify in 2100 or 2300.

Added this is for 2300 and made it clear it is a deviation in  $\Delta\text{GMSL}$

Fig. 3: indicate the units of tuned coefficients.

Units have been added for  $C$  and  $\gamma_T^*$  and the time delay. We’ve also taken the opportunity to update the value of  $p$  on the x-axis as a percentage rather than a fraction for clarity.

Section 3.3: the increased surface mass balance for higher temperatures holds for moderate warming, but for RCP8.5 warming to 2300, there will likely be more ablation by surface melting and the surface mass balance may become negative at some locations (see Kittel et al. 2021, their Fig. 5 where the negative runoff contribution of the grounded-ice SMB starts to significantly increase towards 2100). This is likely somewhat captured by the lower bound of the  $p$  parameter which is well below what is expected from the Clausius-Clapeyron relationship, but this could be briefly discussed.

This is an important point and we are grateful for the paper recommendation. Following a comment from Referee 1 we have now made it clear that we have not used a PDD melt model, and are therefore not imposing any surface melt. We have also added a sentence to the end of Section 3.3 that states that the lower bound of the  $p$  parameter is capable of capturing low rates of total surface mass balance that would occur if there was surface melting under RCP 8.5 forcing, although Kittel et al. 2021 suggest that an increase in surface runoff/negative smb is unlikely to be widespread across the Filchner-Ronne ice shelf in comparison to other regions.

L. 215-221: please provide references, e.g. to IPCC-AR5, and indicate whether the provided warming values refer to the CMIP5 multi-model mean or to the MAGICC emulator.

We have added a reference to the IPCC report and made it clear that these are the multi-model mean estimates presented in the AR5 report.

L. 275: a better or additional reference here would be Favier et al. (2019) in which the box model (“PICO”) was evaluated as a relatively good parameterization: Favier et al. (2019). Assessment of sub-shelf melting parameterisations using the ocean–ice-sheet coupled model NEMO (v3. 6)–Elmer/Ice (v8. 3). *Geosci. Mod. Dev.*, 12(6), 2255-2283.

Thank you for suggesting this paper, we have added it to the text.

L. 280: indicate that this is sea-floor temperature and salinity.

Added

Discussion section: There is a deep uncertainty related to processes that are not represented, e.g. evolution of the position of the calving front, hydrofracturing due to higher surface melt in the future, evolution of ice damage. Some of these processes may play a key role in the future FRIS contribution to sea level, and this should be discussed.

We have added a couple of sentences to the final paragraph of the discussion that highlights these key areas of additional uncertainty in projections of sea level contribution.

### **Response to additional external feedback**

We are grateful for this additional external feedback that raises a number of important points for clarification. Again our responses are below in blue

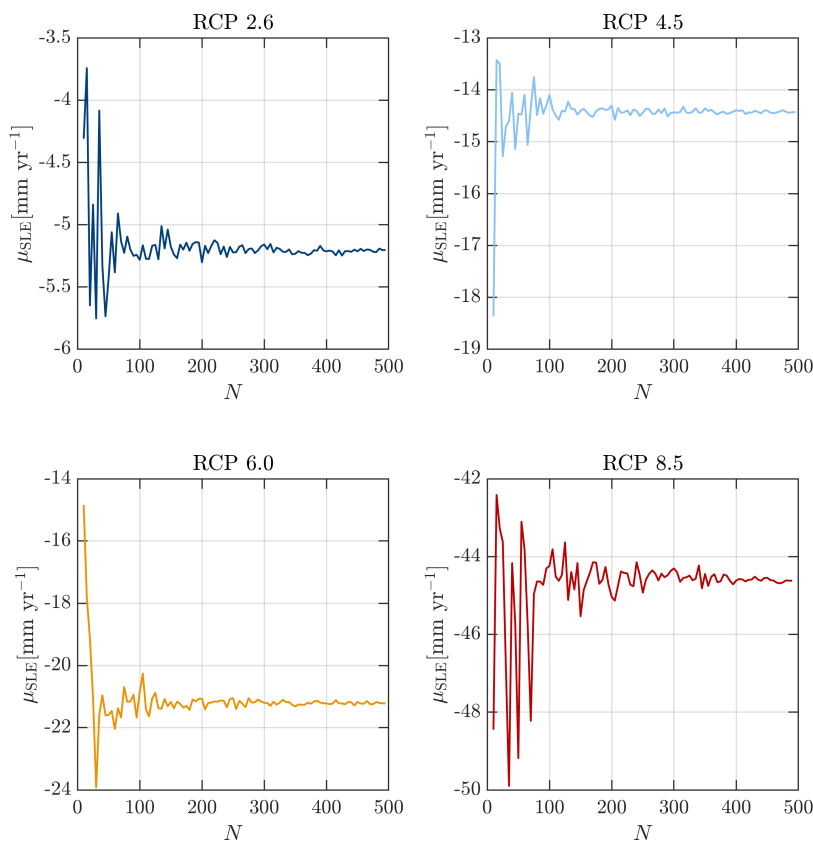
- A single model realisation is used to create the 2300 projections. It would have been more rigorous to use several simulations, in order to test the extremes of plausible scenarios.

While this is true, we do obtain a single climate realisation from the MAGICC simulations between 2100 and 2300 for each RCP scenario, we are still capturing a spread around these projections by imposing error bounds on global mean temperature change (shaded regions in Figure 4). Therefore it is almost as if we have used an ensemble of simulations, which is captured in our parameter  $T$ , that samples a climate realisation from within the shaded uncertainty regions, and is certainly better than using a single projection.

- A Latin hypercube is used to sample 500 parameter values. Why was 500 chosen as the design size ? Has anything been done to check the plausibility of the values or to sample extremes?

We considered a 500 member ensemble to be a sufficiently large ensemble, and beyond that it becomes computationally challenging. We have also tested that the mean and variance of our surrogate models have converged based on the number of samples used in the training set to create the surrogate models. To do this we took the original "training" ensemble, and randomly extracted members from this, in sample sizes of 10 to 500 at intervals of 5 samples, we then created a surrogate model using each of these values for  $N$  (99 additional surrogate models for each RCP scenario). This reveals that  $N = 500$  (or potentially less for some RCP scenarios) is sufficient for the mean and variance of our projections to converge. We've added a sentence into the text and the figure below into the supplement.

To answer the second question, the assumption here is that any of the values within the uncertainty ranges we specify for our input parameters are plausible (see response to final point too). This is because the bounding values for these parameters are informed based on those presented in the literature, which have therefore already been determined as "plausible". It would obviously be interesting to go back and test this further, and in particular, validate our model responses based on observations before using that parameter set in a future simulation. We partly did this for our box model parameters, but agree it could be extended to other parameters. This would make interesting future work.



- Several parameters are given uniform priors without much reasoning. Why was uniform the best choice?

In the absence of better constraints from prior studies or observations, for some parameters, it is not possible for us to make a more informed choice about the priors. As a result we choose not to restrict the sampling in any way, and prescribe only an upper and lower limit, and assume equal probability (uniform priors). It is a whole exercise in itself to determine more informed priors for these parameters based on available data and observations. We did choose to do this for the parameters used in the basal melt parametersation, because we were able to do this efficiently with the box model, and we had good observations in order to constrain the parameters. However, for other parameters, in particular those related to the inversion, determining the values most likely to replicate observations, is still an open question and would require a separate study. In response to a comment by Reviewer 1, we have added a couple of sentences to the discussion that mention uniform priors for  $p$  as a caveat.

- The long tail for RCP8.5 contributions at 2300 is mentioned as being due to certain parameter combinations – what combinations? Are they plausible? That would tell a lot about how much attention should be paid to these upper values.

We could argue that any of the parameter combinations within our parameter space are plausible, given our current understanding of the bounds/uncertainties related to these input parameters. We have made the statement in the text that we believe this long tail to represent large contributions to sea level rise, but is highly unlikely, as it lies outside of the 5-95th percentiles (see Figure 6). However, in hindsight, we think that the original statement in the text may have been a bit misleading, as not only do we not include any follow up, or discussion, of the combinations, but our Sobol indices reveal that the variability in RCP 8.5 contributions is primarily due to variations in  $a$  and is not dependent on specific combinations of parameters. For clarity we have simply removed the statement "certain parameter combinations".

# Quantifying the potential future contribution to global mean sea level from the Filchner-Ronne basin, Antarctica

Emily A. Hill<sup>1,2</sup>, Sebastian H. R. Rosier<sup>2</sup>, G. Hilmar Gudmundsson<sup>2</sup>, and Matthew Collins<sup>1</sup>

<sup>1</sup>College of Engineering, Mathematics and Physical Sciences, University of Exeter, Exeter, United Kingdom

<sup>2</sup>Department of Geography and Environmental Sciences, University of Northumbria, Newcastle Upon Tyne, United Kingdom

**Correspondence:** Emily A. Hill [emily.hill@northumbria.ac.uk](mailto:emily.hill@northumbria.ac.uk)

**Abstract.** The future of the Antarctic Ice Sheet in response to climate warming is one of the largest sources of uncertainty in estimates of future changes in global mean sea level ( $\Delta$ GMSL). Mass loss is currently concentrated in regions of warm circumpolar deep water, but it is unclear how ice shelves currently surrounded by relatively cold ocean waters will respond to climatic changes in the future. Studies suggest that warm water could flush the Filchner-Ronne (FR) ice shelf cavity during the 21st century, but the inland ice sheet response to a drastic increase in ice shelf melt rates, is poorly known. Here, we use an ice flow model and uncertainty quantification approach to project the GMSL contribution of the FR basin under RCP emissions scenarios, and assess the forward propagation and proportional contribution of uncertainties in model parameters (related to ice dynamics, and atmospheric/oceanic forcing) on these projections. Our probabilistic projections, derived from an extensive sample of the parameter space using a surrogate model, reveal that the FR basin is unlikely to contribute positively to sea level rise by the 23rd century. This is primarily due to the mitigating effect of increased accumulation with warming, which is capable of suppressing ice loss associated with ocean-driven increases in sub-shelf melt. Mass gain (negative  $\Delta$ GMSL) from the FR basin increases with warming, but uncertainties in these projections also become larger. In the highest emission scenario RCP 8.5,  $\Delta$ GMSL is likely to range from  $-103$  to  $26$  mm, and this large spread can be apportioned predominantly to uncertainties in parameters driving increases in precipitation (30%) and sub-shelf melting (44%). There is potential, within the bounds of our input parameter space, for major collapse and retreat of ice streams feeding the FR ice shelf, and a substantial positive contribution to GMSL (up to approx. 300 mm), but we consider such a scenario to be very unlikely. Adopting uncertainty quantification techniques in future studies will help to provide robust estimates of potential sea level rise and further identify target areas for constraining projections.

## 1 Introduction

Ice loss from the Antarctic Ice Sheet has accelerated in recent decades (Rignot et al., 2019; Shepherd et al., 2018) and the <sup>c1</sup>evolution of the ice sheet <sup>c2</sup>in response to future climate warming is one of the largest sources of uncertainty for global mean sea level rise. Current projections suggest that the ice sheet may contribute anywhere between  $-7.8$  and  $30$  cm to sea level rise by 2100 under Representative Concentration Pathway (RCP) 8.5 scenario forcing (Seroussi et al., 2020). This large spread of

---

<sup>c1</sup> future

<sup>c2</sup> under

potential sea level rise is primarily due to uncertainties in ocean-driven thinning of ice shelves, which could initiate a positive  
25 feedback of rapid, unstable retreat and ultimate collapse of the the West Antarctic Ice Sheet (Feldmann and Levermann, 2015).

The Filchner-Ronne (FR) basin is a region of Antarctica that has undergone little change in recent decades, and hence has not been the focus of substantial research compared to regions of Antarctica that have already begun to contribute more dramatically to sea level rise. However, the future of this region in response to climate and ocean changes remains highly uncertain. The Filchner-Ronne ice shelf (hereafter FRIS) is the second largest floating ice shelf in Antarctica, spanning approximately  
30  $400 \times 10^3 \text{ km}^2$ , and terminating in the Weddell Sea (Figure 1). Currently the ice shelf discharges approximately  $200 \text{ Gt yr}^{-1}$  (Gardner et al., 2018) of sea level relevant ice mass into the surrounding ocean. Ice from the interior of the Antarctic ice sheet flows into the FRIS primarily via 11 fast-flowing ice streams (Figure 1). These ice streams are marine-based, i.e. their bed topography rests substantially below sea level, which has implications for marine ice sheet instability (Ross et al., 2012). Throughout this paper we refer to the FR basin as the <sup>c1</sup>combined area of the two major drainage basins (Jpp-K, J-Jpp) as  
35 defined by Rignot et al. (2019) that encompass a number of smaller ice-stream catchments that drain into the FRIS.

Current mass loss from the Antarctic Ice Sheet is concentrated in regions where warm circumpolar deep water propagates on the continental shelf (e.g. Amundsen Sea Embayment (ASE): Jacobs et al., 2011; Jenkins et al., 2010; Schmidtko et al., 2014). Warm water in the ASE has been linked to recent ice shelf thinning (Pritchard et al., 2012; Paolo et al., 2015), grounding line retreat (Rignot et al., 2014), and increased ice discharge (Mouginot et al., 2014; Shepherd et al., 2018; Rignot et al., 2019).  
40 In contrast, water entering the FRIS cavity is relatively cold ( $< 0^\circ\text{C}$ ), high-salinity shelf water, and as a result, sub-shelf melt rates are an order of magnitude lower than those in the ASE. The FR basin is also a region of Antarctica that has not undergone significant change during the modern observational period. Over the past four decades (1979–2017), the FR basin has remained relatively stable (accumulation is balanced by discharge) (Rignot et al., 2019), alongside a negligible change ( $1 - 3 \text{ cm yr}^{-1}$ ) in surface elevation (Shepherd et al., 2019) and no significant long-term speed up of the major ice streams (Gudmundsson and  
45 Jenkins, 2009; Gardner et al., 2018).

Recent work suggests that melt rates beneath the FRIS could greatly increase in response to a tipping point in the neighbouring Weddell Sea. Studies have now shown that 21st century changes in atmospheric conditions and sea ice concentration could redirect relatively warm deep water beneath the FRIS via the Filchner trough (Figure 1: Hellmer et al., 2012, 2017; Hazel and Stewart, 2020). This would cause the FR cavity to switch from what is widely referred to as a 'cold-state', to a 'warm-based'  
50 cavity, similar to the ice shelf cavities (e.g. Pine Island and Thwaites) in the ASE. Ultimately, this warm water could be directed towards highly buttressed regions of the ice shelf close to the grounding line (Reese et al., 2018a) via deep cavity bathymetry (e.g. Foundation Ice Stream: Rosier et al., 2018), and dramatically increase melt rates under the FRIS. A loss of resistive stress

---

<sup>c1</sup> *Text added.*

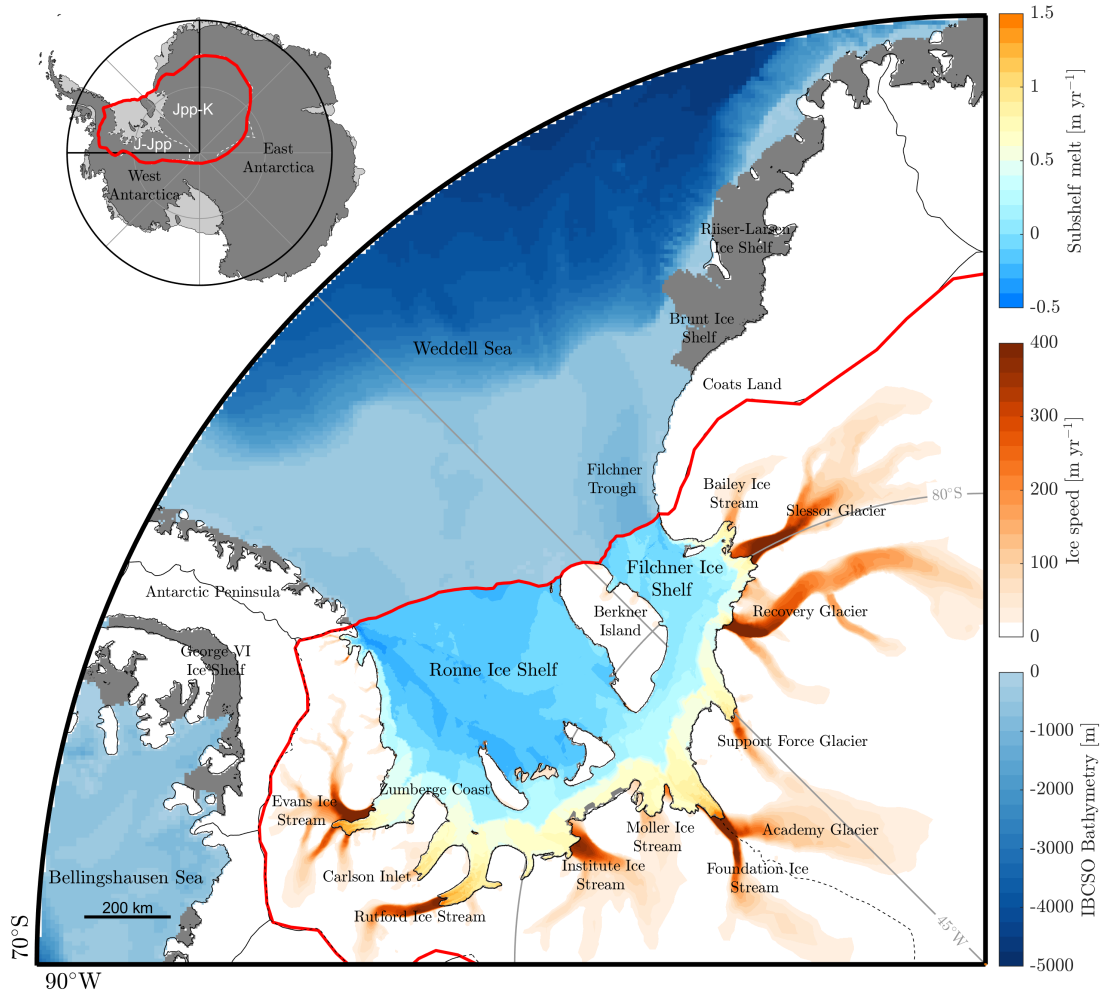


**Figure 1.** Map of Filchner-Ronne region. Our model domain is outlined in red. Orange to red shows model-calculated ice speeds [ $\text{m yr}^{-1}$ ] initialised to observations using a model inversion with  $m = 3$  and  $n = 3$ , over the grounded portion of the catchment. Blue to yellow shading shows sub-shelf melt rates across the Filchner and Ronne ice shelves, using the ocean box melt parameterisation with <sup>c2</sup>sample point estimates for parameters from their probability distributions (see Appendix B). Light to dark blue shading shows sea floor depth from the IBCSO dataset (Arndt et al., 2013). Inset map shows the full extent of our model domain (red) <sup>c3</sup>as well as the drainage basins (Jpp-K, J-Jpp) as defined by Rignot et al. (2019) <sup>c4</sup>in white.

at the grounding line as a result of ocean–induced melt could force dynamic imbalance and grounding line retreat of the ice streams feeding the FRIS.

55 <sup>c5</sup>Most previous studies have only assessed uncertainties in sea level contribution, on an ice sheet wide scale, rather than individual drainage basins (with the exception of Schlegel et al., 2018). <sup>c6</sup>These Antarctic wide ensemble simulations also rely on coarse grid resolution to be computationally feasible, and as a result may not capture small scale processes or accurate grounding line migration relevant on regional scales. Some studies have performed sensitivity experiments to climate–ocean forcing on the FR basin (Cornford et al., 2015; Wright et al., 2014), but we do not know of an uncertainty quantification assessment of the FR region’s potential contribution to sea level rise. A comprehensive uncertainty analysis is needed to fully understand the future of this region of Antarctica should it undergo an increase in sub-shelf melting.

In this paper, we use an uncertainty quantification approach to assess the future of the FR basin to achieve three aims: 1) estimate potential mass change from the FR basin through to the year 2300, 2) quantify the uncertainty associated with mass change projections, and 3) identify parameters in our model or forcing functions that account for the majority of our projection uncertainty and should be priority areas for further research to constrain the spread of future projections. To do this, we integrate an existing suite of uncertainty quantification tools (UQLAB: Marelli and Sudret, 2014) for use with the state-of-art ice flow model Úa (Gudmundsson, 2020). See Figure 2 for a summary of the method used in this paper. The paper is structured as follows: in the following section (2) we introduce the uncertainty methodology used in this paper. In Section 3 we explain the model set-up and input parameters that are propagated through our forward-model. Section 4 presents our probabilistic projections and the results of our sensitivity analysis, which are then discussed in Section 5.

## 2 Uncertainty quantification

Uncertainty quantification can be broadly defined as the science of identifying sources of uncertainty, and determining their propagation through a model or real world experiment with the ultimate goal of quantifying, in probabilistic terms, how likely an outcome or quantity of interest may be.

75 Early estimates of uncertainties in projections of future sea level change from the Antarctic Ice Sheet were derived from sensitivity studies that evaluated a small sample of a parameter space directly in individual ice sheet models (e.g. DeConto and Pollard, 2016; Winkelmann et al., 2012; Golledge et al., 2015; Ritz et al., 2015). Model intercomparison experiments have since been used to quantify uncertainties associated with differences in the implementation of physical processes between models, beginning with idealised set-ups (e.g. MISMIP and MISMIP+ Pattyn et al., 2012; Cornford et al., 2015), and more recently on an ice-sheet scale as part of the ISMIP6 project (Seroussi et al., 2020). Recently, the use of uncertainty quantification techniques has become more common for estimating uncertainties in projections of, for example, sea level rise, based on the current knowledge of uncertainties associated with model parameters or forcing functions (parametric uncertainty) (Edwards et al., 2019; Schlegel et al., 2018; Bulthuis et al., 2019; Aschwanden et al., 2019; Nias et al., 2019; Schlegel et al., 2015;

---

<sup>c5</sup> ~~Despite the FR basin being included in a number of Antarctic wide studies, in most cases with the exception of Schlegel et al., 2018, the sea level rise contribution, and associated uncertainties of individual regions, are not quantified~~

<sup>c6</sup> *Text added.*

Wernecke et al., 2020). This includes techniques that weight model parameters and outputs according to some performance  
 85 measures, to provide a probabilistic assessment of sea level change (Pollard et al., 2016; Ritz et al., 2015). Some of these  
 studies have also drawn upon statistical surrogate modelling techniques such as Gaussian process emulators (Edwards et al.,  
 2019; Pollard et al., 2016; Wernecke et al., 2020) or polynomial chaos expansions (Bulthuis et al., 2019) to mimic the behaviour  
 of an ice-sheet model, and sample a much larger parameter space to make predictions of Antarctic contribution to sea level  
 rise.

90 In this study, we are using a probabilistic approach, in which we are primarily interested in quantifying uncertainties in  
 the forward propagation of input uncertainties that relate to parameters in the model or in the functions used to force climate  
 warming, on a quantity of interest. We make use of the MATLAB based toolbox, UQLab, and the uncertainty quantification  
 framework of Sudret (2007), on which the MATLAB based toolbox is based (Marelli and Sudret, 2014). UQLab includes an  
 extensive suite of tools encompassing all necessary aspects of uncertainty quantification. Here, we summarise the approach  
 95 and tools used in this study (Figure 2) and we refer the reader to the UQLAB documentation (uqlab.com Marelli and Sudret,  
 2014) for further details.

We can think of a physical model ( $\mathcal{M}$ ) as a map from an input parameter space to an output quantity of interest, as

$$Y = \mathcal{M}(X) \tag{1}$$

where our uncertain input parameters are specified as a probabilistic input model ( $X$ ) with a joint probability distribution  
 100 function  $X \sim f_X(x)$ , and  $Y$  is a list of model responses. Using this approach we are able to propagate the uncertainties in the  
 inputs  $X$  to the outputs  $Y$ . We can think of our ice-flow model in the same way,  $\Delta\text{GMSL} = \mathcal{U}_a(X)$ , where  $\Delta\text{GMSL}$  is our  
 model response or quantity of interest. In the following sections we outline eight uncertain input parameters that are represented  
 in  $X$ . These relate to basal sliding and ice rheology (Section 3.2), surface accumulation (Section 3.3) and sub-shelf melting  
 (Section 3.4). Uncertainties in these input parameters are defined in a probabilistic way based on the available information  
 105 (Figure 3). For parameters used to force sub-shelf melt rates, we conducted a separate Bayesian analysis to determine their  
 input parameter probability distributions (see Appendix B).

Quantifying the uncertainty in model outputs due to uncertainty in input parameters or forcings, may require a computation-  
 ally unfeasibly large number of model evaluations. However if, for example, the model response varies slowly as the values  
 of some input parameters are changed, the relationship between model inputs and model outputs may be approximated using  
 110 a much simpler and computationally faster surrogate model. The uncertainty estimation can then be done in a much more  
 computationally efficient way using the surrogate model.

Polynomial chaos expansion (PCE) is a surrogate modelling technique that approximates the relationship between input  
 parameters and output response in an orthogonal polynomial basis. Aside from the work of Bulthuis et al. (2019), PCE surrogate  
 modelling has not yet been used extensively by the glaciological community as a computationally efficient substitute for ice  
 115 sheet models. The truncated PCE,  $\mathcal{M}^{PC}(X)$ , used to approximate the behaviour of our ice sheet model  $\mathcal{M}(X)$  takes the form

$$\mathcal{M}(X) \approx \mathcal{M}^{PC}(X) = \sum_{\alpha \in \mathcal{A}} y_{\alpha} \Psi_{\alpha}(X) \tag{2}$$

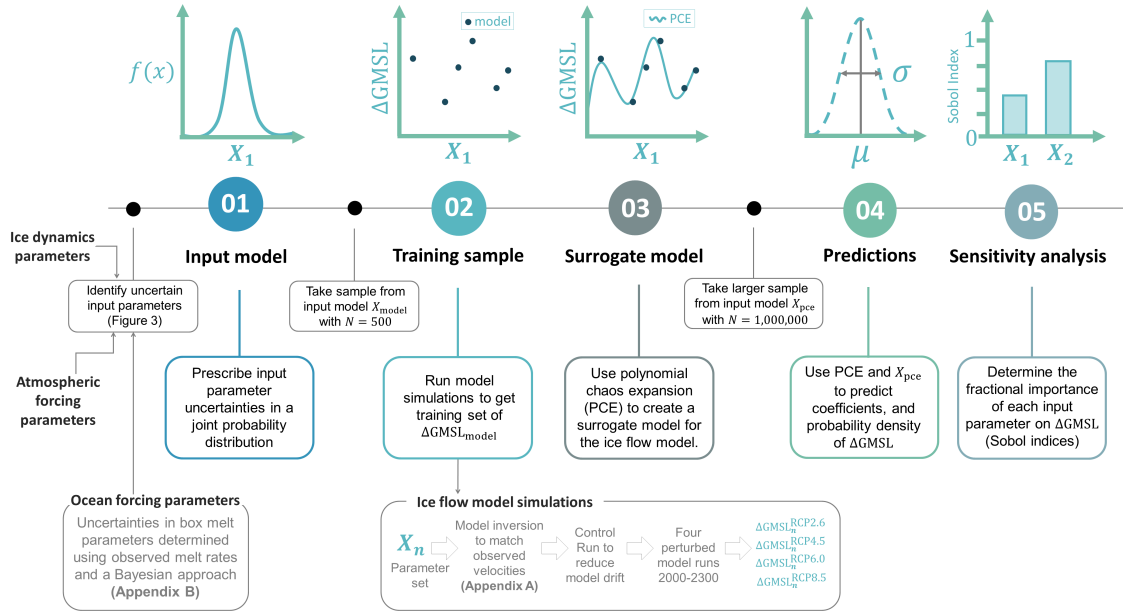


**Figure 2.** Workflow diagram summarising the uncertainty quantification approach used in this study. We first identify uncertain input parameters and represent them in probabilistic framework. A training sample of 500 points is taken from this input parameter space and used as input to an ensemble of simulations in our ice flow model, <sup>c1</sup> [which we hereafter refer to as our "training ensemble"](#). Using this training sample, and the surrogate modelling capabilities in UQLAB we create a polynomial chaos expansion (PCE) that mimics the behaviour of our ice flow model. This allows us to evaluate a much larger sample from our parameter space and these surrogate models are used to derive predictions and probability density functions for changes in global mean sea level ( $\Delta\text{GMSL}$ ). Finally, we use sensitivity analysis to identify the proportional contribution of each input parameter on projection uncertainty.

where  $\Psi_\alpha(X)$  are multivariate polynomials that are orthonormal with respect to the joint input probability density function  $f_X$ ,  $\mathcal{A} \subset \mathbb{N}^M$  is a set of multi-indices of the multivariate polynomials  $\Psi_\alpha$ , and  $y_\alpha$  are the coefficients. Here, our PCEs are calculated using the least angle regression (LAR) algorithm in UQLab (Blatman and Sudret, 2011; Marelli and Sudret, 2019) that solves a least-square minimisation problem. This algorithm iteratively moves regressors from a candidate set to an active set and at each iteration a leave-one-out cross-validation error is calculated. After all iterations are complete, the best sparse candidate basis are those with the lowest leave-one-out error. This is designed to reduce the potential for over-fitting, and reduced accuracy when making predictions outside of the training set. This sparse PCE calculation in UQLab also uses the LOO error for: 1) adaptive calculation of the best polynomial degree based on the experimental design and 2) adaptive q-norm setup for truncation scheme. For further details on the PCE algorithm see Marelli and Sudret (2019). We also outline details on how input uncertainties were propagated through our model to create our PCE in Section 3.5.

Once the surrogate model has been created, the moments of the PCE are encoded in its coefficients where the mean ( $\mu^{PC}$ ) and variance  $(\sigma^{PC})^2$  are as follows

$$\mu^{PC} = \mathbb{E}[\mathcal{M}^{PC}(X)] = y_0 \quad (3)$$

130

$$(\sigma^{PC})^2 = \mathbb{E}[(\mathcal{M}^{PC}(X) - \mu^{PC})^2] = \sum_{\substack{\alpha \in \mathcal{A} \\ \alpha \neq 0}} y_\alpha^2 \quad (4)$$

Our existing PCE surrogate models can additionally be used in a sensitivity analysis to quantify the proportional contribution of parametric uncertainty on projections of  $\Delta$ GMSL. This allows us to identify input parameters where improved understanding is needed to constrain future projections. Here, we are using Sobol indices which are a variance-based method where the model can be expanded into summands of increasing dimension, and total variance in model output can be described as the sum of the variances of these summands.

135

First order indices ( $S_i$ ), often also referred to as "main-effect<sup>c1</sup><sub>S</sub>", are the individual effect of each input parameter ( $X_i$ ) on the variability in the model response ( $Y$ ), defined as:

$$S_i = \frac{\text{Var}[\mathbb{E}(Y|X_i)]}{\text{Var}(Y)} \quad (5)$$

140

Total Sobol indices ( $S_i^T$ ) are then the sum of all Sobol indices for each input parameter and encompass the effects of parameter interactions. Values for Sobol Indices are between 0 and 1, where large values of  $S_i$  indicate parameters that strongly influence the projections of global mean sea level. If  $S_i \approx S_i^T$  then it can be assumed that the effect of parameter interactions is negligible.

145

These Sobol indices can be calculated analytically from our existing PCEs, by expanding portions of the polynomial that depend on each input variable to directly calculate parameter variance using the PCE coefficients. Each of the summands of the PCE can be expressed as

$$f_{\mathbf{v}}(x_{\mathbf{v}}) = \sum_{\alpha \in \mathcal{A}_{\mathbf{v}}} y_\alpha \Psi_\alpha(X) \quad (6)$$

Due to the orthonormality of the basis, the variance of our truncated PCE reads as

$$\text{Var}[\mathcal{M}^{PC}(X)] = \sum_{\substack{\alpha \in \mathcal{A} \\ \alpha \neq 0}} y_\alpha^2 \quad (7)$$

$$\text{Var}[f_{\mathbf{v}}(x_{\mathbf{v}})] = \sum_{\substack{\alpha \in \mathcal{A}_{\mathbf{v}} \\ \alpha \neq 0}} y_\alpha^2 \quad (8)$$

150

The first order Sobol indices in Equation 5 are then calculated as the ratio between the two above terms.

---

<sup>c1</sup> Text added.

### 3 Methods

#### 3.1 Ice-flow model

Here we use the vertically integrated ice-flow model  $\dot{U}a$  (Gudmundsson, 2020) to solve the ice dynamics equations using the shallow-ice stream approximation (SSTREAM), also commonly referred to as the shallow-shelf approximation (SSA) and the 'shelfy-stream' approximation. (MacAyeal, 1989).  $\dot{U}a$  has been used in previous studies on grounding line migration and ice shelf buttressing and collapse (De Rydt et al., 2015; Reese et al., 2018b; Gudmundsson et al., 2012; Gudmundsson, 2013; Hill et al., 2018) and model results have been submitted to a number of intercomparison experiments (Pattyn et al., 2008, 2012; Levermann et al., 2020; Cornford et al., 2020).

Our model domain extends across the two major drainage basins that feed into the FRIS (Figure 1). Within this domain, we generated a finite-element mesh (Figure S1) with  $\sim 92,000$  nodes and  $\sim 185,000$  linear elements using the Mesh2D Delaunay-based unstructured mesh generator (Engwirda, 2015). Element sizes were refined based on effective strain rates and distance of the grounding line and <sup>c1</sup>have a maximum size of 27 km, a median size of 2 km, and a minimum size of 660 m. Within a 10 km distance of the grounding line elements are 3 km, and refined further to 900 m within a distance of 1.5 km. <sup>c2</sup> Outside of our uncertainty analysis, we tested the sensitivity of our results to mesh resolution by repeating our median and maximum  $\Delta$ GMSL simulations under RCP 8.5 forcing, and dividing or multiplying the aforementioned element sizes by two. Our results are largely insensitive to the mesh resolution, with a percentage deviation <sup>c3</sup>in  $\Delta$ GMSL of only 3% <sup>c4</sup>by 2300. Finally, we linearly interpolated ice surface, thickness and bed topography from BedMachine Antarctica v1 (Morlighem et al., 2020) onto our model mesh. We initialise our model to match observed velocities using an inverse approach (see Section 3.2 and Appendix A).

During forward transient simulations,  $\dot{U}a$  allows for fully implicit time integration, and the non-linear system is solved using the Newton-Raphson method.  $\dot{U}a$  includes automated time-dependent mesh refinement, allowing for high mesh resolution around the grounding line as it migrates inland. We also impose a minimum thickness constraint <sup>c5</sup>of 30 m using the active-set method to ensure that ice thicknesses remain positive. Throughout all simulations our calving front remains fixed in its originally prescribed position. At the end of each forward simulation we calculate the final change in global mean sea level ( $\Delta$ GMSL) as the ice volume above flotation that will contribute to sea level change based on the area of the ocean (Goelzer et al., 2020).

#### 3.2 Basal sliding and ice rheology

There are two components of surface glacier velocities; internal deformation and basal sliding.  $\dot{U}a$  uses inverse methods to optimise these velocities components based on observations by estimating the ice rate factor ( $A$ ) in Glen's flow law and basal

---

<sup>c1</sup> Text added.

<sup>c2</sup> ~~ranging from 900 m close to the grounding line, and in the shear margins, to a maximum of 50 km further inland.~~

<sup>c3</sup> Text added.

<sup>c4</sup> Text added.

<sup>c5</sup> Text added.

180 slipperiness parameter ( $C$ ) in the sliding law. This section introduces uncertainties related to the exponents of the flow law and basal sliding law, whereas details of the inverse methodology are included in Appendix A.

Glen's flow law (Glen, 1955) is used to relate strain rates and stresses as a simple power relation

$$\dot{\epsilon}_{ij} = A\tau_e^{n-1}\tau_{ij} \quad (9)$$

where  $\dot{\epsilon}_{ij}$  are the elements of the strain rate tensor,  $\tau_e$  is effective stress (second invariant of the deviatoric stress tensor),  $\tau_{ij}$  are the elements of the deviatoric stress tensor,  $A$  is the temperature dependent rate factor, and  $n$  is the stress exponent.

This stress exponent ( $n$ ) controls the degree of non-linearity of the flow law and most ice flow modelling studies adopt  $n = 3$ , as it is considered applicable to a number of regimes (See review in: Cuffey and Paterson, 2010). However, experiments reaching high-stresses (Kirby et al., 1987; Goldsby and Kohlstedt, 2001; Treverrow et al., 2012), or analysing borehole measurements, and ice velocities (e.g. Gillet-Chaulet et al., 2011; Cuffey and Kavanaugh, 2011; Bons et al., 2018) have suggested that  $n > 3$ . It is also possible that at low stresses, the creep regime may become more linear  $n < 3$  (Jacka, 1984; Pettit and Waddington, 2003; Pettit et al., 2011), which is supported by ice shelf spreading rates  $n = 2 - 3$  (Jezek et al., 1985; Thomas, 1973). While it can be considered that  $n = 3$  is appropriate in most dynamical studies, the exact numerical value is not known and it appears plausible that it can range between 2 and 4. To capture the uncertainty in the stress exponent we take  $n \in [2, 4]$  and sample continuously from a uniform distribution within this range (Figure 3).

195 Basal sliding is considered the dominant component of surface velocities in fast flowing ice streams. The Weertman sliding law is defined as

$$\tau_b = C^{-1/m} \|\mathbf{v}_b\|^{1/m-1} \mathbf{v}_b \quad (10)$$

where  $C$  is a basal slipperiness coefficient and  $\mathbf{v}_b$  the basal sliding velocity. The Weertman sliding law typically captures hard-bed sliding, in which case  $m = n$  and is normally set equal to 3 (Cuffey and Paterson, 2010). However, using different values for  $m$  alters the non-linearity of the sliding law, and can thus be used to capture different sliding processes, i.e. viscous flow for  $m = 1$  and plastic deformation for  $m = \infty$ . There are limited in situ observations of basal conditions, and the value of  $m$  relies on numerical estimates of basal sliding based on model fitting to observations.

A number of studies have tested different values of  $m$  to fit observations of grounding line retreat or speedup at Pine Island Glacier (Gillet-Chaulet et al., 2016; Joughin et al., 2010; De Rydt et al., 2021). These studies show that  $m = 3$  can underestimate observations, and more plastic like sliding ( $m > 3$ ) is needed in at least some parts of the catchment to replicate observations (Joughin et al., 2010; De Rydt et al., 2021). This uncertainty in the value of  $m$  can ultimately affect projections of sea level rise (Ritz et al., 2015; Bulthuis et al., 2019; Alevropoulos-Borrill et al., 2020) by altering the length and time taken for perturbations (e.g. ice shelf thinning or grounding line retreat) to propagate inland.

While additional sliding laws have been proposed and are now implemented within a number of existing ice flow models, in this study we use the Weertman sliding law, as it remains the most common. This narrows the parameter space, allowing us to fully integrate the influence of  $m$  on projections of future sea level rise into our uncertainty assessment (by performing

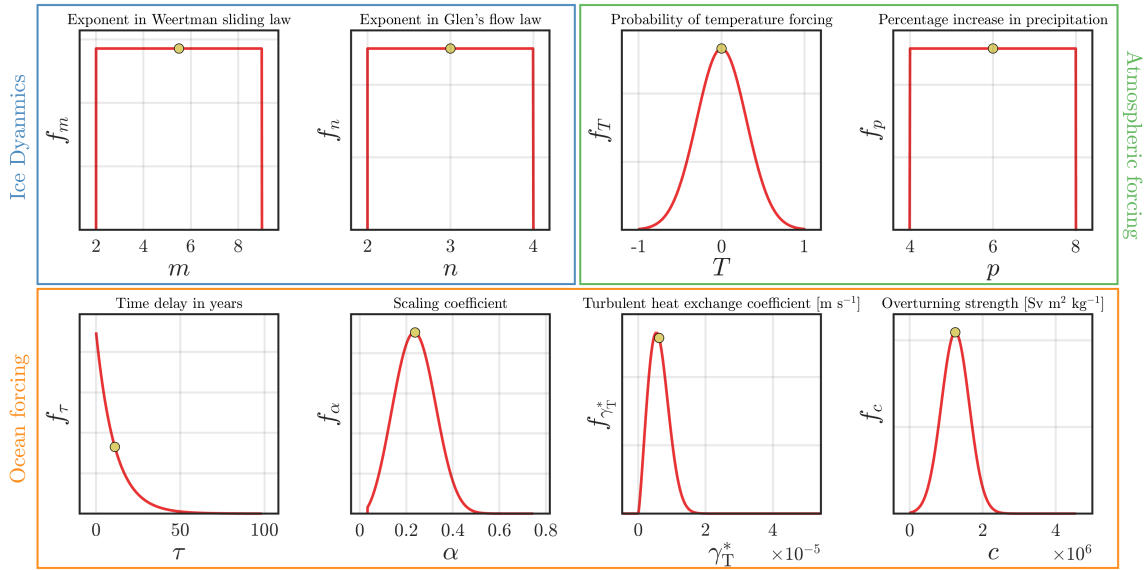


**Figure 3.** Probability distributions for uncertain parameters included in our analysis, grouped by ice dynamics (blue rectangle), atmospheric forcing (green rectangle), and ocean forcing (orange rectangle). For each parameter, x-axes show the parameter bounds, and red lines show the probability distribution functions. Yellow circles show the <sup>c1</sup>sample point estimates for each of our parameters. The distributions of the four ocean forcing parameters are outputs from our Bayesian analysis (Appendix B) in which we optimized the parameter distributions using observations melt beneath the Filchner-Ronne ice shelf.

an inverse model run prior to each perturbed run, see Section 3.5). This is an advancement over previous Antarctic wide studies, that given domain size have no choice but to invert the model for a handful of different  $m$  values prior to uncertainty propagation (e.g. Bulthuis et al., 2019; Ritz et al., 2015). To capture uncertainty in  $m$  and to sample from a range of possible  
215 methods of basal slip, we take  $m \in [2, 9]$  and sample from a uniform distribution (Figure 3).

### 3.3 Surface accumulation

To capture uncertainties in future climate forcing, we use projections from four Representative Concentration Pathways (RCPs) presented in the Fifth Assessment Report of the Intergovernmental Panel on Climate Change (IPCC). These pathways capture plausible changes in anthropogenic greenhouse gas emissions for the 21st and 22nd centuries. RCP 2.6 is a strongly mitigated  
220 scenario, <sup>c2</sup>and multi-model mean estimates from the IPCC report (IPCC, 2014) <sup>c3</sup>project a global temperature increase of less than  $2^\circ\text{C}$  above pre-industrial levels by 2100, and is the goal of the 2016 Paris Agreement. Two intermediate scenarios (RCP 4.5 and RCP 6.0) represent global temperature increases of  $\sim 2.5^\circ\text{C}$  and  $\sim 3^\circ\text{C}$  with reductions in emissions after 2040 and

<sup>c2</sup> Text added.

<sup>c3</sup> Text added.

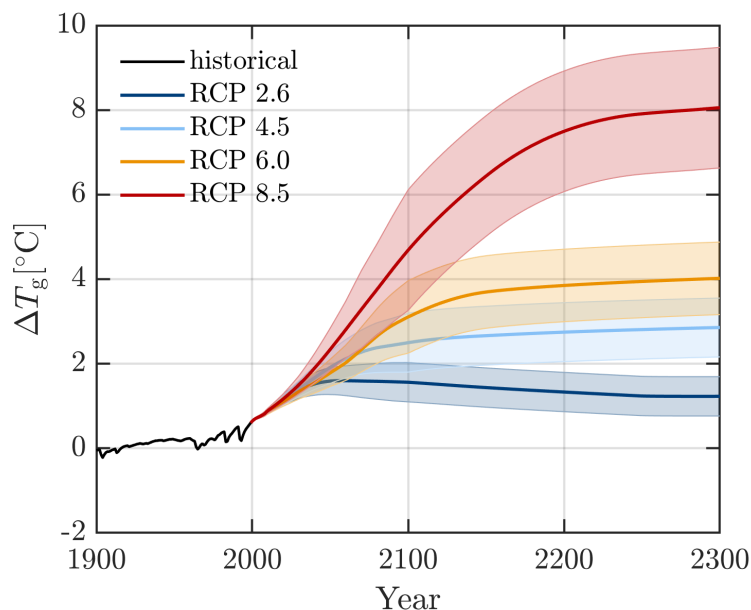


**Figure 4.** Changes in global mean temperatures ( $\Delta T_g$  [°C]) relative to pre-industrial levels (1860 to 1899) for four Representative Concentration Pathways (RCPs) 2.6 (blue), 4.5 (green), 6.0 (yellow), 8.5 (pink). Shading shows uncertainty regions between the 25th and 75th percentiles.

2080 respectively (IPCC, 2014). Finally, RCP 8.5 projects a global temperature increase of  $\sim$  <sup>c4</sup>4.5°C by 2100 and is now often referred to as an "extreme" or "worst-case" climate change scenario.

225 Global mean temperature changes ( $\Delta T_g$ ) from 1900 to 2300 relative to pre-industrial (1860–99) were obtained from the atmosphere–ocean general circulation model emulator MAGICC6.0 (live.magicc.org; Meinshausen et al. (2011)). For each RCP scenario we obtain 600 (historically-constrained) model simulations between 2000 and 2100 (see Meinshausen et al. (2009) for details on the probabilistic set-up). We then use the ensemble median and uncertainty bounds within a "very likely" range between the 25th and 75th percentiles. To extend the record to 2300, we use a single model realisation, using the default  
 230 climate parameter settings used to produce the RCP greenhouse gas concentrations for each RCP scenario (Meinshausen et al., 2009) , and keep the upper and lower bounds constant from 2100 to 2300 (Figure 4). Uncertainty in projections from 2100 to 2300 may well be larger, but we choose not to make an assumption on how errors will propagate up to 2300. Global temperatures from MAGICC 6.0 were also used in the Antarctic linear response model inter-comparison (LARMIP-2) experiment (Levermann et al., 2020) and are consistent with projections used in other Antarctic wide simulations (Bulthuis et al., 2019;  
 235 Golledge et al., 2015).

Following the work of a number of previous studies (e.g. Pattyn, 2017; Bulthuis et al., 2019; DeConto and Pollard, 2016; Garbe et al., 2020), global temperature changes ( $\Delta T_g$ ) are used to force annual changes in surface mass balance through our

forward-in-time simulations, by prescribing changes in surface temperature ( $T_{\text{air}}$ ) and precipitation ( $P$ ) as follows:

$$T_{\text{air}} = T_{\text{obs}}^{\text{air}} - \gamma(s - s_{\text{obs}}) + \Delta T_{\text{g}} \quad (11)$$

240

$$P = A_{\text{obs}} \times \exp(p \cdot (T_{\text{air}} - T_{\text{obs}}^{\text{air}})) \quad (12)$$

where  $T_{\text{obs}}^{\text{air}}$  and  $A_{\text{obs}}$  are surface temperatures and accumulation rates from RACMO2.3 respectively (Van Wessem et al., 2014). Temperature changes through time are corrected for changes in surface elevation ( $s$ ) from initial observations ( $s_{\text{obs}}$ ), using a lapse rate of  $\gamma = 0.008^\circ\text{C m}^{-1}$  (Pattyn, 2017; DeConto and Pollard, 2016), and subsequently used to force changes in precipitation using an expected percentage increase in precipitation ( $p$ ) per degree of warming (Aschwenden et al., 2019). This captures the rise in snowfall expected with the increased moisture content of warmer air, suggested by climate models (e.g. Palerme et al., 2017; Frieler et al., 2015). <sup>c1</sup>Here, we do not implement a positive degree day surface melt model. While it is possible that RCP 8.5 forcing in particular, could cause enhanced surface melting in some regions of Antarctica, due to the southern location of the Filchner-Ronne ice shelf, surface melt and runoff are unlikely to outweigh increases in snowfall in the high warming scenario (Kittel et al., 2021).

250

To capture further uncertainties associated with atmospheric forcing, we introduce two uncertain parameters into our analysis, 1) a scaling factor to select a temperature realisation between the 25th and 75th percentiles of the ensemble median temperature for each RCP scenario (Figure 4) and 2) uncertainty in the expected changes in precipitation across the Antarctic ice sheet with increased air temperatures.

255

First, instead of only using the ensemble median change in temperature for each RCP scenario, we capture the spread within each forcing scenario by incorporating a temperature scaling parameter ( $T$ ) as follows:  $\Delta T_{\text{g}}(n) = \Delta T_{\text{g}}^{\text{median}} + T \cdot T_{\text{g}}^{\text{err}}$ , where for each RCP scenario  $\Delta T_{\text{g}}^{\text{median}}$  is the median,  $\Delta T_{\text{g}}^{\text{err}}$  is the distance either side of the median within the 25th and 75th percentiles, and  $\Delta T_{\text{g}}(n)$  is the resultant temperature realisation used to force both surface accumulation ( $P$ ) and ocean temperature (see Section 3.4). We assume that there is decreasing likelihood of temperature profiles further away from the median, and so prescribe a Gaussian distribution for  $T$  between  $-1$  (25th percentile) and  $1$  (75th percentile) and centered around 0 (median: Figure 3).

260

Secondly, we capture uncertainty associated with precipitation by varying the amount by which precipitation increases per degree of warming ( $p$ ). While it is generally accepted that accumulation will increase with future warming, the value of  $p$  remains uncertain. Snow accumulation could prevent runaway ice discharge from the Antarctic ice sheet, which means that parameterisations of precipitation increase with warming have implications for accurate projections of mass change across the ice sheet. Previous studies using ice core records, historical global climate model (GCM) simulations, and future GCM simulations as part of the CMIP5 ensemble, have estimated anywhere between 3.7–9% increase in Antarctic accumulation per degree of warming (Krinner et al., 2007, 2014; Gregory and Huybrechts, 2006; Bengtsson et al., 2011; Ligtenberg et al., 2013; Frieler et al., 2015; Palerme et al., 2017; Monaghan et al., 2008). To capture this range of possible values for ( $p$ ) we sample

265

---

<sup>c1</sup> *Text added.*

270 from  $p \in [4, 8]$  and make no assumption of the distribution (likelihood) of the value of  $p$  within this range by sampling from a uniform distribution (Figure 3). <sup>c2</sup>While the lower bound of this range sits below what is expected from the Clausius-Clapeyron relationship, it is able to capture low rates of surface mass balance that could occur with some (albeit limited) increases in surface runoff and melt under RCP 8.5 forcing.

### 3.4 Sub-shelf melt

275 Ice shelf thinning due to ocean-induced melt can reduce buttressing forces on grounded ice and accelerate ice discharge. Such feedbacks may already be taking place in parts of West Antarctica. However, future changes in ocean conditions remain uncertain, owing to poor understanding and the challenges of modelling interactions between global atmospheric warming and ocean circulation/temperature changes (Nakayama et al., 2019; Thoma et al., 2008). In particular, the likelihood that the Filchner-Ronne ice shelf cavity will be flushed with modified warm deep water in the future is unclear (Hellmer et al., 2012).

280 To parameterise basal melting beneath the ice shelf, we use an implementation of the PICO ocean box model (Reese et al., 2018a) for use in Úa, which we hereafter refer to as the ocean box model. This provides a computationally feasible alternative to fully coupled ice-ocean simulations for large ensemble analysis, <sup>c1</sup>which is more physically based than simple depth dependent parameterisations (e.g. Favier et al., 2014) <sup>c2</sup>and has been shown to provide similar results to coupled simulations under future climate forcing scenarios (Favier et al., 2019). The basic overturning circulation in ice shelf cavities is captured using a series of ocean boxes, calculated based on their distance from the grounding line. The overturning flux  $q$  is then calculated as 285 the density difference between the far-field ( $p_0$ ) and grounding line ( $p_1$ ) water masses using a constant overturning strength parameter ( $c$ ). The melt parameterisation also includes a turbulent heat exchange coefficient  $\gamma_T^*$  that controls the strength of melt rates by varying the heat flux across the ice-ocean boundary. For a detailed description of the physics of the PICO box model, see Reese et al. (2018a). To calculate sub-shelf melt rates, the box model requires inputs of <sup>c3</sup>sea-floor temperature 290 ( $T_{\text{ocean}}$ ) and salinity ( $S$ ) on the continental shelf to drive the ocean cavity circulation. We use  $S = 34.65$  psu and the initial observed ocean temperature for the Weddell Sea  $T_{\text{obs}}^{\text{ocean}} = -1.76^\circ\text{C}$  from Schmidtko et al. (2014) which was proposed for use in PICO (Reese et al., 2018a). For the FR basin we use five ocean boxes, and only apply sub-shelf melting to nodes that are fully afloat (no connecting grounded nodes) to avoid overestimating grounding line retreat (Seroussi and Morlighem, 2018).

To force changes in sub-shelf melt rates using RCP forcing, we update the far-field ocean temperature ( $T_{\text{ocean}}$ ) through time 295 with an ocean temperature anomaly:

$$T_{\text{ocean}} = T_{\text{obs}}^{\text{ocean}} + \Delta T_o \quad (13)$$

It is often assumed that atmospheric temperature changes  $\Delta T_g$  can be translated to ocean temperature changes  $\Delta T_o$  using some scaling factor ( $\alpha$ ) (Maris et al., 2014; Golledge et al., 2015; Levermann et al., 2014, 2020). Here, we use the linear scaling

---

<sup>c2</sup> Text added.

<sup>c1</sup> ~~but~~

<sup>c2</sup> Text added.

<sup>c3</sup> Text added.

proposed in Levermann et al. (2020) which additionally includes a time delay  $\tau$  to capture the assumed time lag between  
300 atmospheric and subsurface ocean warming.

$$\Delta T_o = \alpha \cdot \Delta T_g(t - \tau) \quad (14)$$

To obtain suitable values for  $\alpha$  and  $\tau$ , Levermann et al. (2020) used 600 atmospheric temperature realisations (also from MAG-  
ICC6.0 simulations) and ocean temperatures from 19 CMIP5 models (Taylor et al., 2012) to derive the relation between global  
305 surface temperatures and subsurface ocean warming by computing the correlation coefficient ( $\alpha$ ) and time delay between the  
signals ( $\tau$ ). The values proposed are consistent with  $\alpha \approx 0.25$  used in a number of other Antarctic wide simulations (Bulthuis  
et al., 2019; Golledge et al., 2015; Maris et al., 2014). However, given the spread of values depending on the choice of CMIP5  
model, no single value for either  $\alpha$  and  $\tau$  can be chosen with confidence, and it is instead appropriate to sample from parameter  
probability distributions.

We identify a further two uncertain parameters in the ocean box model that additionally control the strength of sub-shelf  
310 melt. These are the turbulent heat exchange coefficient  $\gamma_T^*$  and the strength of the overturning circulation  $c$ . Values for these  
parameters presented in Reese et al. (2018a) have been optimised to present day ocean temperatures and observations of  
melt rates for a circum-Antarctic set-up. While upper and lower bounds for these parameters have also been proposed (Reese  
et al., 2018a; Olbers and Hellmer, 2010), little information exists on the likelihood of parameter values within these ranges,  
particularly for different regions of Antarctica, with varying ocean conditions.

315 For the four parameters that control the sub-shelf melt rates ( $\alpha$ ,  $\tau$ ,  $\gamma_T^*$  and  $c$ ) we decided to constrain their uncertainty (prob-  
ability distributions) using a Bayesian approach. Using the a priori information on the distributions for  $\alpha$  and  $\tau$  (Levermann  
et al., 2020) and possible upper and lower bounds for  $\gamma_T^*$  and  $c$  from Reese et al. (2018a); Olbers and Hellmer (2010), along-  
side observed sub-shelf melt rates from Moholdt et al. (2014), we derive optimised posterior probability distributions for use as  
input to our uncertainty propagation. The details of this are outlined in Appendix B, and the resultant probability distribution  
320 functions for these parameters are shown in Figure 3.

### 3.5 Propagating uncertainty

In this section we explain how uncertainties in the input parameters introduced in the previous sections are propagated through  
our model to obtain projections of global mean sea level (Figure 2). We began by generating an experimental design (training  
set) for the surrogate model. An input parameter sample of 500 points was extracted from the parameter space using Latin  
325 hypercube sampling. <sup>c1</sup>This sample was determined to be sufficient in size such that the mean  $\Delta$ GMSL <sup>c2</sup>had converged for  
each RCP surrogate model (see Figure S3). <sup>c3</sup>Using each training sample we then evaluate the ice flow model to generate model  
responses. For each sample point we perform six model runs. First, we perform a model inversion following the procedure  
outlined in Appendix A using the selected values for  $m$  and  $n$ . The resulting optimised fields of  $C$  and  $A$  are then input

---

<sup>c1</sup> Text added.

<sup>c2</sup> Text added.

<sup>c3</sup> At each training point

into five forward-in-time simulations, four based on different RCP scenarios and one control run, all of which run from 2000  
330 (nominal start year) to 2300.

Experience has shown that our model (similar to others e.g. Bulthuis et al., 2019; Schlegel et al., 2018) undergoes a period  
of model drift at the start of the simulation, characterised by a slowdown and thickening of many of the ice streams in our  
domain <sup>c1</sup>amounting to between 80 and 100 mm of negative contribution to  $\Delta\text{GMSL}$ . We found model drift to be similar  
between parameter sets, but was affected by the basal boundary conditions from our inversion. Hence, rather than specify a  
335 single baseline for the entire experimental design, we perform a control simulation for each set of basal boundary conditions.  
This control run uses selected values of  $m$  and  $n$  and inverted fields of  $C$  and  $A$  but holds all other input parameters fixed to  
their <sup>c2</sup>sample point estimates, as well as using a constant temperature forcing. Each control run is followed by four forward  
runs, one for each RCP forcing scenario, in which surface accumulation and sub-shelf melt rates are updated at annual intervals  
based on global temperature changes (Figure 4). The final calculated change in global mean sea level for each RCP scenario is  
340 with respect to the preceding control run ( $\Delta\text{GMSL}_{\text{rcp}} - \Delta\text{GMSL}_{\text{ctrl}}$ ). For our 500 member <sup>c3</sup>training ensemble we perform  
500 model inversions, and 2500 forward simulations.

Model responses ( $\Delta\text{GMSL}$ ) and input parameter sample  $X = x_1, \dots, x_N$  are used to train four surrogate models (one for each  
RCP scenario). This is done using the Polynomial Chaos module in UQLab (Marelli and Sudret, 2019) using the LAR algorithm  
previously described in Section 2. We allow the LAR algorithm to choose a PCE with a degree anywhere between 3 and 15 and  
345 q-norm between 0.1 and 1. Predictions (mean and variance) of  $\Delta\text{GMSL}$  are then directly extracted from each surrogate model.  
To estimate the accuracy of our PCE predictions and calculate quantiles we use bootstrap replications. We use 1000 replications  
( $B$ ) each with the same number of sample points as the original experimental design (500) to create an additional set of  $B$  PCEs  
and associated responses. Quantiles (5th and 95th) were extracted from the bootstrap evaluations (see Supplementary Figure  
S2). To assess the performance of our surrogate model, we generated an additional and independent validation sample of 20  
350 <sup>c4</sup>sample points in the parameter space, evaluated for each RCP scenario (total of 80 perturbed simulations). <sup>c5</sup>We then calcu-  
late the root mean square error (RMSE) between validation responses  $Y_{\text{val}}$  to those calculated by each surrogate model ( $Y_{\text{PCE}}$ )  
using the same validation input parameter sample  $X_{\text{val}}$ . Predictions made by the surrogate models are close to the responses by  
our ice-flow model and <sup>c6</sup>have a maximum RMSE error of 2.3 mm for our RCP 8.5 surrogate model (Supplementary Figure  
S2).

---

<sup>c1</sup> *Text added.*

<sup>c2</sup> *Text added.*

<sup>c3</sup> *Text added.*

<sup>c4</sup> *Text added.*

<sup>c5</sup> *Text added.*

<sup>c6</sup> *Text added.*

	2100	2200	2300
RCP 2.6	-3.2(-6.4, 0.113)	-5.05(-13.2, 3.86)	-5.49(-19.1, 9.57)
RCP 4.5	-4.99(-8.96, -0.975)	-11(-22.7, 1.87)	-15.1(-36.1, 9.7)
RCP 6.0	-5.41(-9.51, -1.3)	-15.4(-29.7, 0.204)	-22.3(-49.6, 11.1)
RCP 8.5	-8.39(-14.1, -2.99)	-30.2(-55.2, -3.42)	-48(-103, 26)

**Table 1.** Contribution to global mean sea level [mm] at years 2100, 2200 and 2300. The first number is the median projection and values in brackets are 5–95% confidence intervals

## 355 4 Results

### 4.1 Projections of sea level rise from FR basin

We begin by presenting probabilistic projections of global mean sea level change from the Filchner-Ronne basin for four RCP scenarios. These projections were derived from surrogate models that were trained with our 500 member <sup>c7</sup>[training](#) ensemble of forward-in-time ice flow model simulations. We then evaluated these surrogate models with a 1,000,000 point sample <sup>c8</sup>[\(generated using Latin hypercube sampling\)](#) from our input parameter space to derive model responses, and calculated probability distributions using kernel density (Figure 5).

Our projections indicate it is most likely that the FR basin will undergo limited change or contribute negatively to global mean sea level by the year 2300. Under the lowest warming scenario (RCP 2.6: 0.77 – 1.7°C),  $\Delta$ GMSL is limited, ranging between -19.1 mm (5th) and 9.57 mm (95th percentiles: Table 1). The probability distribution (Figure 5) takes a near-to-normal shape, with a median projection close to zero (-5.49 mm), but has a weak positive skew of 0.16 (calculated using the moment coefficient of skewness), with a tail extending towards a maximum sea level contribution of  $\sim$  50 mm. Projections of  $\Delta$ GMSL under the medium warming scenarios RCP 4.5 and 6.0 range from -36.1 to 9.7 mm and -49.6 to 11.1 mm respectively (Table 1). These distributions are more positively skewed than RCP 2.6 (skewness coefficients of 0.29 and 0.39 respectively), with tails extending towards  $\sim$  100 mm of global sea level rise (Figure 5). Extreme warming leads to the greatest uncertainty in projections, which range from -103 to 26 mm under RCP 8.5 (Table 1). The median projection indicates a greater negative contribution to sea level rise under higher warming. However, the probability distribution is asymmetric, with a long-tail (high positive skew = 0.77), that decreases exponentially away from the median and reaches a maximum  $\Delta$ GMSL of 332 mm (Figure 5). This long-tail represents the potential for low-probability, but high magnitude contributions to sea level rise <sup>c1</sup>.

375 As our surrogate modelling is based around a single quantity of interest ( $\Delta$ GMSL) it does not allow us to evaluate temporal changes in ice loss directly. Figure 6 instead presents projections through time from our 500 member <sup>c2</sup>[training](#) ensemble alongside the final  $\Delta$ GMSL from each surrogate model (PCE). We also generate two additional surrogate models for each

<sup>c7</sup> Text added.

<sup>c8</sup> Text added.

<sup>c1</sup> ~~under certain parameter combinations~~

<sup>c2</sup> Text added.

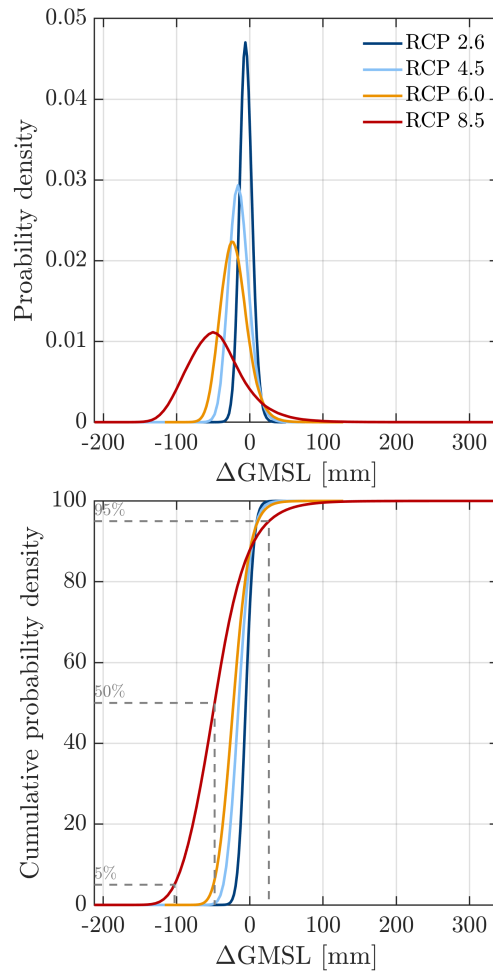


**Figure 5.** Probability density (top) and cumulative probability density (bottom) for projections of change in global mean sea level ( $\Delta\text{GMSL}$ ) in millimetres by the year 2300 under four RCP emissions scenarios. Dashed lines show the 5, 50 and 95th percentiles for the highest emission scenario RCP 8.5

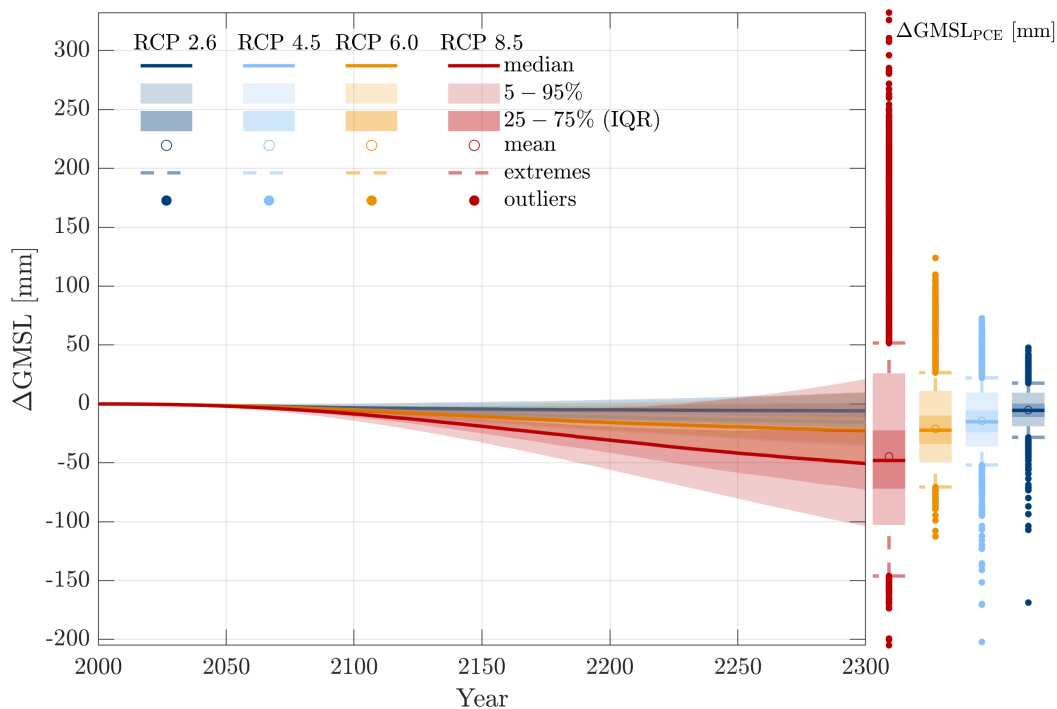


**Figure 6.** Projections of changes in global mean sea level ( $\Delta\text{GMSL}$ ) from 2000 and 2300 from our <sup>c1</sup>training ensemble of ice flow model simulations. Dark shading is the interquartile range (IQR) defined between the 25th and 75th percentiles. Lighter shading shows 5th–95th percentiles. Box plots show the projections from the surrogate models ( $\Delta\text{GMSL}_{\text{PCE}}$ ) for each RCP scenario at 2300. Extreme values are located at 1.5 times the interquartile range away from the 25th and 75th percentiles. Values outside of these extreme bounds are considered to be outliers.

RCP scenario at years 2100 and 2200 (Table 1) to evaluate projections at these time intervals, and identify the temporal importance of parameters on projection uncertainty (see Section 4.2 and Figure 7).

380 Both Table 1 and Figure 6 show that the contribution to  $\Delta\text{GMSL}$  and associated uncertainties increase through time. Within the next 100 years (up to 2100) we project little change in ice mass from the FR basin. This constitutes a small negative contribution to sea level rise of  $< 10$  mm in all warming scenarios (Table 1), with a maximum range of  $-14.1$  to  $0.11$  mm. By 2200 the spread of  $\Delta\text{GMSL}$  has diverged based on warming scenario, with little change under limited forcing (RCP 2.6 =  $-5.05$ ), and a greater negative contribution under with higher warming ( $-30.2$  in RCP 8.5). Between 2200 and 2300  
 385 uncertainties increase dramatically in all warming scenarios, particularly in RCP 8.5. Box plots on Figure 6 show the projections generated from our surrogate model in 2300 alongside our ice flow model <sup>c2</sup>training ensemble. <sup>c3</sup>This shows that the probability distributions in the most likely range between 5-95% generated from our surrogate models are largely similar to those found

<sup>c2</sup> Text added.

<sup>c3</sup> Text added.

from our training ensemble in 2300. However, we note that the tail<sup>c4</sup>s of these distributions, in particular for RCP 8.5, extend<sup>c5</sup> substantially beyond the maximum  $\Delta\text{GMSL}$  <sup>c6</sup>shown from our <sup>c7</sup>training ensemble <sup>c8</sup>alone (150 mm). While, this is expected  
390 with more extensive sampling of our parameter space, we test the feasibility of  $\Delta\text{GMSL} = 332$  mm, by taking the parameter values that led to this, and re-evaluating the "true" ice flow model. This gives a slightly lower value of  $\Delta\text{GMSL} = 250$  mm, but one that is still considerably higher than in our original <sup>c9</sup>training ensemble despite its relatively large size ( $N = 500$ ). <sup>c10</sup>This demonstrates the benefits of our surrogate modelling approach, as it was able to capture the possibility of more extreme sea level rise scenarios that were not exposed by the original sample. Recalculating the surrogate model for RCP 8.5 including this  
395 "extreme" sample point, reduces the maximum contribution to sea level rise to 288 mm.

## 4.2 Parametric Uncertainty

In this section we present the results of our sensitivity analysis, in which we determine how uncertainties in our input parameters (parametric uncertainty) impact our projections of  $\Delta\text{GMSL}$ . To do this, first order Sobol indices were decomposed from each of our PCE models (four RCP forcing scenarios) and for three timesteps: 2100, 2200 and 2300, which are presented in Figure  
400 7. We additionally assessed the individual parameter to projection relationship, by re-evaluating our surrogate model for each parameter, while all other parameters were held at their <sup>c1</sup>sample point estimates (see Supplementary Figure S4).

By 2300 (dark shaded bars in Figure 7) uncertainties in our four ocean forcing parameters collectively have the greatest fractional contribution to the uncertainty in our projections of global mean sea level contribution. This ranges from 60% in RCP 8.5 to 75% for RCP 2.6. Projection uncertainty in all RCP scenarios is primarily driven by ocean temperature forcing,  
405 and the value of  $\alpha$  used to scale atmospheric to ocean temperatures. Uncertainties attributed to  $\alpha$  appear to increase both with warming scenario and through time. In all RCP scenarios, fractional uncertainty associated with  $\alpha$  increases from 2100 to 2300 (light shaded bars in Figure 7), coincident with an increase in the spread of  $\Delta\text{GMSL}$  contribution (Figure 6). In 2100,  $\alpha$  has a greater impact on projection uncertainty in the lower warming scenario. However, by 2300, the fractional uncertainty is greatest in RCP 8.5, accounting for almost half of projection uncertainty (0.44) compared to 0.34 in RCP 2.6. Re-evaluating the  
410 surrogate models varying only the value of  $\alpha$  reveals a quadratic dependency of  $\Delta\text{GMSL}$  on the value of the scaling coefficient (Supplementary Fig S4), which is consistent with the quadratic sensitivity of sub-shelf melt rates to ocean temperature forcing observed for the FR ice shelf cavity by Reese et al. (2018a). Under extreme warming (RCP 8.5), this quadratic relation becomes stronger, and variability in  $\alpha$  alone can cause  $\Delta\text{GMSL}$  to range between  $-86$  and  $73$  mm by 2300. Under all RCP warming scenarios the value of  $\alpha$  contributes to a greater range of  $\Delta\text{GMSL}$  than any other parameter (Supplementary Fig S4), and  
415 encompasses almost all of the 5–95% spread of projections (Table 1).

---

<sup>c4</sup> Text added.

<sup>c5</sup> s

<sup>c6</sup> Text added.

<sup>c7</sup> Text added.

<sup>c8</sup> Text added.

<sup>c9</sup> Text added.

<sup>c10</sup> highlighting the benefits of our surrogate modelling approach

<sup>c1</sup> Text added.

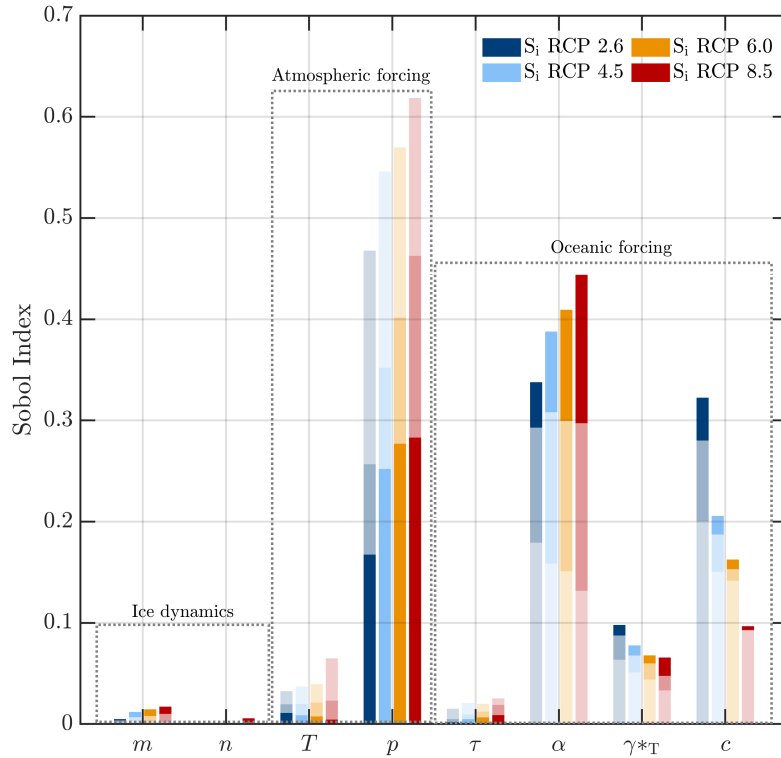


**Figure 7.** First order Sobol indices, i.e. the fractional contribution of each input parameter on the uncertainty in our projections of  $\Delta\text{GMSL}$ , for each RCP forcing scenario. Dark shading shows the Sobol indices for  $\Delta\text{GMSL}$  in 2300. Two lighter shading colours represent Sobol indices at years 2100 and 2200, to show the variability in parameter importance through time.

Of our two ocean box model parameters, overturning strength ( $c$ ) accounts for more projection uncertainty than the turbulent heat exchange coefficient ( $\gamma_T^*$ ) in all warming scenarios. This is consistent with the theory that sub-shelf melting at large and cold-cavity ice shelves is predominantly driven by overturning strength (Reese et al., 2018a). The fractional importance of  $c$  has the greatest variability between forcing scenarios than any other parameter. Unlike  $\alpha$ , uncertainty associated with  $c$  decreases with warming, from 0.32 in RCP 2.6 to 0.1 for RCP 8.5 (Figure 7). The importance of the overturning strength,  $c$ , also increases with time, which is most pronounced in lower warming scenarios, e.g. RCP 2.6 where  $\alpha$  and  $c$  are similar by 420 decreases with warming, from 0.32 in RCP 2.6 to 0.1 for RCP 8.5 (Figure 7). The importance of the overturning strength,  $c$ , also increases with time, which is most pronounced in lower warming scenarios, e.g. RCP 2.6 where  $\alpha$  and  $c$  are similar by 425 similar trend exists for uncertainties associated with  $\gamma_T^*$ ; greater importance for lower warming scenarios and in all scenarios, increasing importance with time. However, in contrast to  $c$ , there is a greater relative increase in the Sobol index for the highest warming scenario (RCP8.5) from 2100 to 2300; the importance of  $\gamma_T^*$  doubled from 0.033 to 0.066 versus only a 54% increase

in RCP 2.6. This suggests that as the FR ice shelf transitions to warm cavity conditions ( $\sim 2^\circ\text{C}$  in RCP 8.5) the heat exchange in the turbulent boundary layer may become a more important driver of sub-shelf melt than under colder conditions.

430 Atmospheric forcing parameters account for the second largest proportion of uncertainty in  $\Delta\text{GMSL}$  by 2300. This is primarily driven by variability in the percentage increase in precipitation per degree of warming ( $p$ ), and to a lesser extent the temperature scaling parameter ( $T$ ). At all time intervals (2100, 2200, 2300), projection uncertainty attributed to  $p$  is largest based on warming scenario. Unlike  $\alpha$ , Sobol indices for  $p$  decrease through time, which is asynchronous to increased uncertainty in  $\Delta\text{GMSL}$  contribution (Figure 6). In 2100,  $p$  accounts for over half of projection uncertainty in all scenarios (except  
435 RCP 2.6) reaching a maximum of 0.62 in RCP 8.5.  $p$  remains the dominant parameter in 2200 for higher warming scenarios, but for RCP 2.6 the Sobol index for  $p$  decreases to 0.26, less than both  $\alpha$  and  $c$ . By 2300, the fractional importance of  $p$  is  $< 0.3$  and lower than  $\alpha$  for all four warming scenarios. Evaluating the surrogate model (at year 2300) for  $p$  only, reveals a linear dependency on the value of  $p$ , where, as expected, increases in precipitation lead to a decrease in the contribution to GMSL, or in this case a greater negative contribution to GMSL (Supplementary Figure S4). In RCP 8.5,  $p$  alone contributes to  
440 between  $-8$  and  $-80$  mm of  $\Delta\text{GMSL}$  (Supplementary Figure S4). This suggests that even with a limited ( $p = 4\%$ ) increase in precipitation, and fixed melt rates, the FR basin is unlikely to contribute positively to  $\Delta\text{GMSL}$ . However, in RCP 2.6, increased accumulation with  $p < 0.05$  does not outweigh mass loss associated with sub-shelf melting and could lead to a small positive contribution to sea level rise.

Finally, uncertainties in our ice dynamical parameters relating to the non-linearity in the sliding ( $m$ ) and flow ( $n$ ) laws used  
445 in our model, have a limited contribution to uncertainties in our projections of  $\Delta\text{GMSL}$  (Figure 7). The combined contribution of these parameters by 2300 under all warming scenarios (0.02 in RCP8.5) is an order of magnitude less than uncertainties associated with atmospheric and oceanic forcing (see Supplementary Figure S5 for Sobol Indices for just  $m$  and  $n$ ). Of the two parameters,  $m$  accounts for the most uncertainty in  $\Delta\text{GMSL}$ , which is unsurprising given that basal sliding is likely to be the dominant component of surface velocities of the fast-flowing ice streams feeding the FR ice shelf. Despite low values of the  
450 Sobol indices, we note that uncertainties in both  $m$  and  $n$  increase with time and the strength of the temperature perturbation (Supplementary Figure S5). Increasing the values of  $m$  and  $n$  in isolation, reduces the negative contribution to  $\Delta\text{GMSL}$ , i.e. less mass gain (Supplementary Fig S4). In both cases, a stronger non-linearity in the ice flow ( $n$ ), or more plastic like flow ( $m$ ), allows for faster delivery of the ice to the grounding line in response to a perturbation.

### 4.3 Partitioned Mass Change

455 Our Sobol indices reveal that the percentage change in precipitation and ocean temperature scaling are the main drivers of uncertainty in changes in global mean sea level. To further examine the relative importance of precipitation and sub-shelf melt parameters on mass change in the FR basin, <sup>c1</sup>[we take our training ensemble and](#) partition components of mass balance (accumulation and discharge) using the input-output method. We calculated the integrated input accumulation ( $P$ ) across the grounded area and the total integrated discharge ( $D$ ) output across the grounding line with respect to our control runs. These

---

<sup>c1</sup> *Text added.*

460 mass balance components, as well as total mass change ( $M = P - D$ ), are shown for the low (RCP 2.6) and high (RCP 8.5) warming scenarios in Figure 8) and for intermediary scenarios in Supplementary Figure S6.

Mass change under the lowest warming scenario (RCP 2.6) closely follows the temperature anomaly trend and appears primarily driven by increases (and subsequent decreases) in accumulation with warming. In the first 50 years, mass balance increases to 12.6 (6.56 – 18.6) Gt yr<sup>-1</sup> (where values in brackets here and in the remainder of this section are 5–95%). This  
465 is primarily due to an increase in accumulation at a rate of 15.2 Gt yr<sup>-1</sup> in 2050, which is offset by a limited increase in discharge across the grounding line (2.5 Gt yr<sup>-1</sup>) during this period. Between 2050 and 2100 accumulation remains constant and discharge increases, which consequently reduces the rate of total mass gain. Uncertainties associated with accumulation are greater than those for discharge during this period (Figure 8c), which is consistent with the high contribution of the percentage increase in precipitation on projection uncertainty in 2100 (Figure 7). The rate of mass gain continues to decrease after 2100,  
470 alongside a reduction in the temperature perturbation in RCP 2.6, and decelerating accumulation. During this period, discharge across the grounding line stabilises at a median of 10 Gt yr<sup>-1</sup>, but the uncertainty range increases dramatically to –8 to 26 Gt yr<sup>-1</sup>, which coincides with an increasing importance of parameters relating to sub-shelf melt from 2200 to 2300 (Figure 7). By 2300 this drives the mass balance towards zero, at which accumulation is approximately balanced by ice discharge.

Under RCP 8.5 forcing the spread of mass change in 2300 is driven by anomalies in ice discharge. During the first 150  
475 years, surface accumulation steadily increases at an average rate of 50 Gt yr<sup>-1</sup>, which is consistent with increased temperature forcing of 6.4°C. During this period, increases in discharge lag that of accumulation, averaging only 9.6 Gt yr<sup>-1</sup>, which can partly be explained by the prescribed time delay between atmospheric and oceanic warming ( $\tau$ : Equation 14). Hence, it appears likely that total mass balance will remain positive up to 2150, as no parameter combinations (c<sup>1</sup>[training](#) ensemble members) are able to sufficiently increase ice discharge above that of accumulation. Consistent with other forcing scenarios, uncertainties  
480 in accumulation are also greater than those associated with discharge, which corresponds to greater projection uncertainty attributed to  $p$  up to 2200 (Figure 7).

After 2150, the rate of temperature increase is reduced, which leads to a reduction in surface accumulation, that plateaus at ~ 140 (86 – 202) Gt yr<sup>-1</sup> between 2200 and 2300. Despite a limited change in temperature (+1.6°C) between 2150 and 2300 (relative to 2000 to 2150), discharge continues to increase linearly from 31 to 92 Gt yr<sup>-1</sup>. Simultaneously, uncertainties  
485 in discharge increase substantially and span 0.05 – 0.76 mm yr<sup>-1</sup> (5–95th percentiles) of sea level equivalent volume in 2300. This suggests that the atmospheric temperature anomaly itself becomes less important than the amount by which atmospheric temperatures are scaled to ocean warming, i.e. the value of  $\alpha$ , where variability in  $\alpha$  alone accounts for most of the range of sea level contribution (Figure 7 and Supplementary Figure S4). Indeed, the spread of total mass change ( $M$ ) closely follows the uncertainties in ice discharge, where it is possible, albeit unlikely, that certain combinations of parameters (within the 5–95th  
490 percentiles) allow for mass imbalance ( $P < D$ ) and a positive contribution to sea level.

Variability in ice discharge alone also reveals the spread of potential positive contribution to sea level rise that would have occurred in our simulations if surface accumulation had remained unchanged. To explore this, we rerun our median simulation under RCP 8.5 forcing using the same parameter values, but keep surface mass balance fixed at it's initial value. This reveals

---

<sup>c1</sup> *Text added.*

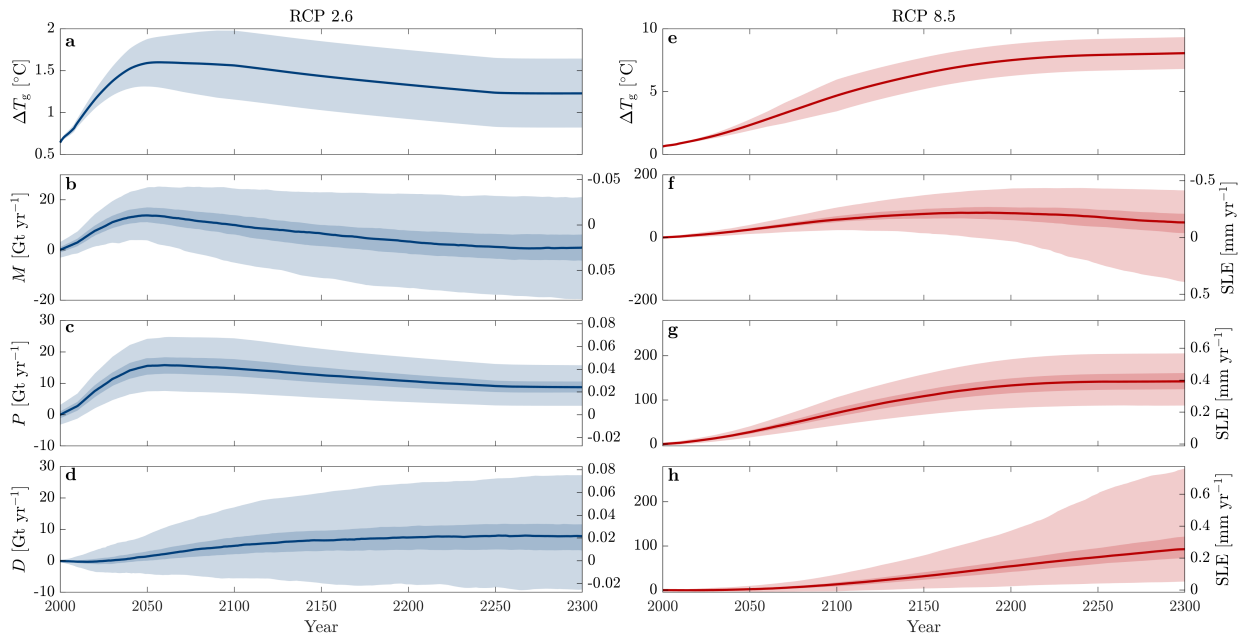


**Figure 8.** Projected temperature changes and mass balance changes for RCP 2.6 (left panels, blue lines) and RCP 8.5 (right, red) between 2000 and 2300 from our <sup>c1</sup>training ensemble. Uncertainties are shown between 5 and 95% in light shading and between 33 and 66% in dark shading **a, e**) Global temperature anomalies, **b, f**) Change in the rate of total mass change ( $M$ ) in  $\text{Gt yr}^{-1}$  calculated as  $P - D$  **c, g**) Change in rate of accumulation integrated over the grounded area ( $P$   $\text{Gt yr}^{-1}$ ) with respect to our control runs ( $P_{\text{rcp}} - P_{\text{ctrl}}$ ). **d, h**) Change in the rate of ice discharge integrated across the grounding line ( $D$   $\text{Gt yr}^{-1}$ ) calculated with respect to our control runs ( $D_{\text{rcp}} - D_{\text{ctrl}}$ )

that increases in sub-shelf melt alone would contribute to 84 mm of global mean sea level rise (as opposed to  $-50$  mm), and  
 495 highlights the important and compensating effect accumulation has on the sign of our sea level projections.

#### 4.4 Grounded Ice Loss

In this section we explore the changes in grounded area throughout our simulations to see how our projections of mass change correspond to the retreat of the grounding line. Figure 9 presents changes in grounded area with respect to the control runs (a) and grounding line positions from <sup>c2</sup>members of our training ensemble closest to our 5, 50 and 95% percentile projections of  
 500  $\Delta\text{GMSL}$  from our surrogate models (b) for RCP 8.5, while additional RCP scenarios are shown in Supplementary Figures S7-S9.

Despite the negative contribution to  $\Delta\text{GMSL}$  likely under all warming scenarios (50th percentiles: Table 1), our results show that these median projections correspond to simulations that all experience a reduction in grounded area by 2300 (Figure 9 and Supplementary Figures S7-S9). In all scenarios there is limited grounding line retreat in the next 100 years (up to 2100),

<sup>c2</sup> ensemble members

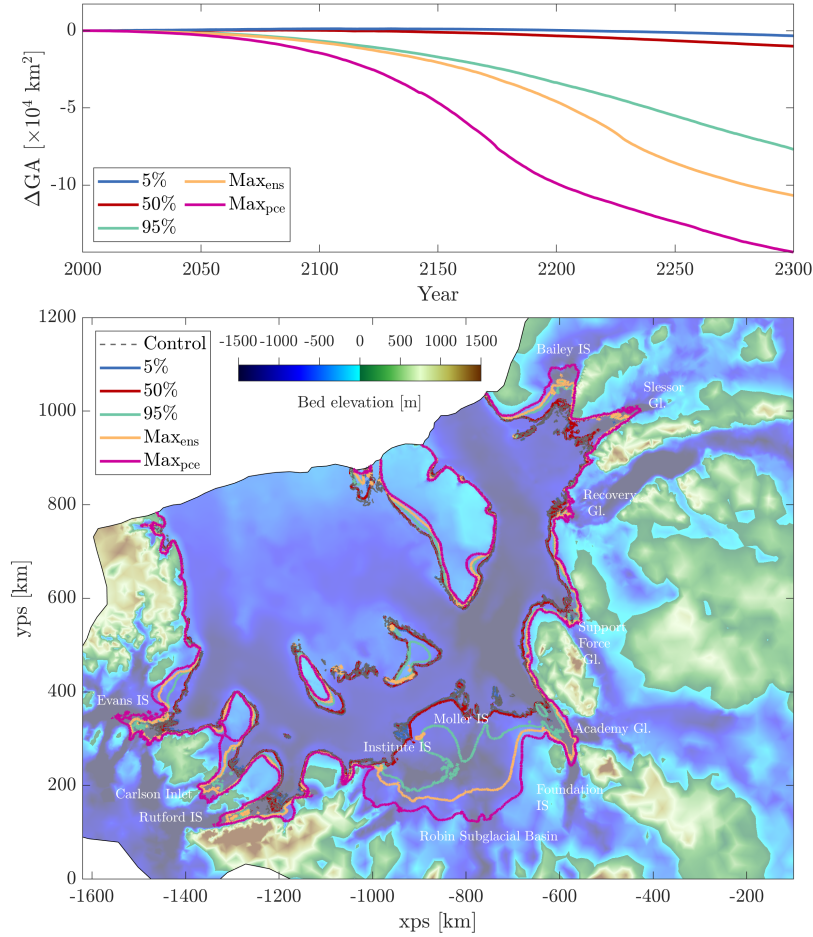


**Figure 9.** Changes in grounded area and grounding line position for RCP 8.5. Top panel shows change in grounded area ( $\Delta GA$  calculated as  $GA_{\text{rcp}} - GA_{\text{ctrl}}$ ) in  $\times 10^4 \text{ km}^2$ . Coloured lines represent the 5th, 50th and 95th percentiles of the projections of  $\Delta \text{GMSL}$  rather than the percentiles of the change in grounded area itself. However, they are generally close to the grounded area results. Lower panel shows the FR basin and bed elevation in metres above (green to brown) and below (light to dark blue) sea level. Coloured lines show grounding line positions from our [c3 training](#) ensemble [c4](#) that lie closest to our percentiles (5, 50 and 95%) from our surrogate model projections, with respect to control runs (dashed grey lines). Two additional grounding line positions are shown; the maximum  $\Delta \text{GMSL}$  from our [c5 training](#) ensemble (orange) and the maximum  $\Delta \text{GMSL}$  from our surrogate model (magenta), which we evaluated separately to our initial [c6 training](#) ensemble of simulations.

505 amounting to only  $-716 \text{ km}^2$  ( $-4800$  to  $2050 \text{ km}^2$ : 5–95%) change in grounded area in RCP 8.5. After 2150, grounded area decreases more rapidly, and the spread of change in grounded area increases within each forcing scenario. This coincides with the timing of a reduction in the rate of accumulation and increases in the rate of grounded ice discharge (Figure 8). This is particularly the case in RCP 8.5 (Figure 9), where more substantial ungrounding coincides with a sharp increase in uncertainty in ice discharge in 2200 and the increasing importance of sub-shelf parameters on projection uncertainty (Figure 7). This indicates that parameters controlling melt rates are responsible for the spread of grounded ice loss via variations in sub-shelf melt applied close to the grounding line. Ultimately this drives the long positive tail of projections of sea level rise contribution ( $\Delta\text{GMSL}$ : Figure 5).

While median projections for all RCP scenarios experience a loss of grounded area by 2300, in the lower warming scenarios (RCP 2.6 and RCP 4.5) this is relatively limited ( $< 800 \text{ km}^2$ ), with the exception of some retreat of the Möller and Institute Ice Streams (Supplementary Figures S7–S9). This suggests that these ice streams are prone to some ungrounding even with limited increases in sub-shelf melting. The likelihood of retreat and complete collapse of these ice streams increases dramatically with warming (RCPs 6.0 and 8.5). In RCP 8.5 perturbations become large enough for possible (but less likely) retreat of additional regions, in particular the Rutford and Evans Ice Streams draining into western part of the Ronne Ice Shelf and some retreat of ice streams feeding the Filchner Ice Shelf (Figure 9). Our separate additional simulation that validated the upper end of sea level projections from our surrogate model ( $\Delta\text{GMSL} = 250 \text{ mm}$ ) shows that there is potential within our parameter space (beyond our initial ensemble) for the grounding line to retreat much further inland (Figure 9). This is characterised by runaway retreat of Möller and Institute ice streams, likely due to being topographically unconfined and rested upon a retrograde bed below sea level (Figure 9). This suggests that increases in sub-shelf melt with climate warming, have the potential to reduce ice shelf buttressing and force substantial grounded ice loss.

## 525 5 Discussion

Here, we have used an uncertainty quantification approach to assess the spread of future changes in global mean sea level ( $\Delta\text{GMSL}$ ) contribution from the Filchner-Ronne region of Antarctica under different RCP emissions scenarios. We have taken a large and extensive sample of parameter space using a novel surrogate modelling approach, and our results show it is highly likely that, within the bounds of our input parameter space,  $\Delta\text{GMSL}$  from the FR basin will be negative. Under RCP 2.6 forcing, during which atmospheric temperatures increase by  $2^\circ\text{C}$  (Figure 4: in line with the targets of the Paris agreement), this region is likely to remain close to balance (accumulation  $\approx$  discharge) and contribute to  $-19.1$  to  $9.57 \text{ mm}$  (5–95%) of sea level rise by 2300. Under higher warming scenarios, projections of sea level rise become increasingly negative, but the uncertainties in these projections also increase dramatically. In the highest warming scenario (RCP 8.5), the FR basin could contribute anywhere between  $-103$  to  $26 \text{ mm}$  (5–95%) to global mean sea level. Our projections are predominantly negative due to the mitigating effect of increased accumulation with warming on sub-shelf melt driven increases in ice discharge.

Increases in precipitation across the Antarctic ice sheet, are known to have an important mitigating effect on the contribution to global sea level rise (Medley and Thomas, 2019; Winkelmann et al., 2012). Unlike other parts of West Antarctica, the

Weddell Sea showed a strong accumulation trend during the 20th century (Medley and Thomas, 2019), and limited change in dynamic ice discharge towards the end of the century (Rignot et al., 2019). Our simulations show that continued increases in accumulation during the 21st century, driven by warming, can outweigh slow increases in ice discharge associated with sub-shelf melting (Figure 8). This may be enough to stabilise some of the major ice streams, in particular the Institute and Möller (see 50% line in Figure 9). In most cases, mass gain continues through to 2300, despite increases in the rate of ice discharge and slow-down in the accumulation trend, both of which are not enough to switch to mass loss/positive  $\Delta$ GMSL by 2300. We continued our median RCP 8.5 simulation for a further 200 years with forcing held at 2300, and found that total mass balance (accumulation – discharge) remained positive (mass gain) by 2500. These findings are consistent with previous regional modelling studies which showed that when applying both accumulation and sub-shelf melt anomalies, it is possible for accumulation to suppress the effects of increased sub-shelf melt and keep the FR basin close to balance (Wright et al., 2014; Cornford et al., 2015). This is in contrast to Antarctic wide simulations that do not impose changes in surface accumulation through time (Ritz et al., 2015; Schlegel et al., 2018) and hence project greater ice loss and sea level rise contribution from this region. Overall, our results demonstrate that the FR basin is particularly sensitive to future accumulation changes, which are capable of stabilising this region in response to climate-warming.

Despite the important role that precipitation plays in suppressing ice loss from the FR basin, our sensitivity analysis reveals that the percentage increase in precipitation per degree of warming  $p$ , is the second largest contributor (approx 30% in RCP 8.5) to uncertainties in our projections. Hence, we can identify the representation of accumulation changes with warming in ice-sheet models as a target area for further research, in order to better constrain projections of sea level contribution. However, modelling future precipitation trends is challenging and CMIP5 models themselves show large temporal and spatial variability in projected precipitation trends with warming (Tang et al., 2018; Palerme et al., 2017; Rodehacke et al., 2020). Despite this, it has been assumed that there is a general correlation between precipitation and temperature anomalies. As a result, temperature scaling of precipitation (as used in this study) is a common approach in ice sheet modelling, most of which use a Clausius–Clapeyron relation, equivalent to a 5% spatially uniform increase in precipitation (Golledge et al., 2015; Gregory and Huybrechts, 2006; Garbe et al., 2020; DeConto and Pollard, 2016). But, as we have shown here, small variations in  $p$  can have a large effect on the spread of  $\Delta$ GMSL projections, and better constraints on the value of  $p$  are needed.

<sup>c1</sup>Sampling from an uncertainty distribution for  $p$  has been valuable to capture the spread of future accumulation change predicted in a warming climate, however, one caveat to this is the use of uniform priors. In the absence of additional constraints, we cannot make a more informed choice on the uncertainty distribution of  $p$ , but it is possible that this leads to a greater spread, or skewed distribution of accumulation changes, with respect to those predicted by CMIP GCMs. Validating these parameterisations to climate model predictions should be the focus of future work. Recent work by Rodehacke et al. (2020) <sup>c2</sup>has made improvements towards Antarctic estimates for  $p$ , and found that the assumed correlation/or lack thereof between temperature and precipitation anomalies, has strong regional differences, which may invalidate the use of a <sup>c3</sup>spatially invariant value for

---

<sup>c1</sup> Text added.

<sup>c2</sup> sought to improve

<sup>c3</sup> simple, uniform scaling

570  $p$ . Instead they propose spatially variable values of  $p$  across the Antarctic Ice Sheet. Over the FRIS, they showed  $p = 4 - 6\%$ , which is consistent with values used in this study, but may reach up to 10% in inland regions of the FR basin (Rodehacke et al., 2020). Thus, using a spatially <sup>c4</sup>invariant value for  $p$ , may lead to under or over estimates of precipitation across the catchment. This is even more important when conducting Antarctic wide simulations, and future studies should move towards using a spatially variable value for  $p$ , or ultimately conduct coupled atmosphere–ocean–ice-sheet simulations.

575 Our probabilistic projections have show that a negative  $\Delta\text{GMSL}$  is most likely from the FR basin. Nonetheless, uncertainties associated with our input parameters reveal that it is also possible within our parameter space for the FR basin to contribute positively to sea level rise. This occurs predominantly under RCP 8.5 forcing, where the the long tail of the projections in Figure 5 reflects these more "extreme" (maximum of 332 mm by 2300) yet unlikely contributions to  $\Delta\text{GMSL}$ . Hence, it is possible for sub-shelf melt to increase enough to outweigh 21st century accumulation, by forcing substantial increases in ice  
580 discharge (Figure 8), and un-grounding of the ice streams feeding the FRIS (Figure 9). These high-magnitude contributions to sea level rise are characterised by the rapid retreat of the lightly-grounded Möller and Institute ice streams, which, once initiated, continues unabated across the Robin subglacial basin throughout our simulations (maximum GMSL simulation: Figure 9). Additional retreat occurs predominantly in the ice streams feeding the Ronne ice shelf (Evans and Rutford Ice streams and Carlson Inlet), suggesting that these regions are likely to be the dominant contributors to future sea level rise.  
585 There is also some potential for un-grounding in the ice streams feeding the Filchner ice shelf, but this is less than elsewhere in the region (Figure 9). Retreat of the grounding line in our simulations is consistent with the magnitude and spatial pattern of retreat simulated in other studies in response to increased ocean–driven melt rates, with comparable projections of sea level rise contribution (approx 150–160 mm) to the high-end of our results (up to 300 mm) (Schlegel et al., 2018; Wright et al., 2014; Cornford et al., 2015).

590 Greater variability in ice discharge from the 22nd century onwards (Figure 8), coincides with an increase in the spread of our projections, suggesting that sub-shelf melt could strongly influence the regions potential contribution to sea level rise. Indeed, our sensitivity analysis clearly reveals that ocean forcing parameters are the dominant component of uncertainties in our projections of sea level contribution from the FR basin (Figure 7). This sensitivity corroborates the well established theory that ocean forcing and the impact on sub-shelf melt rates, is a dominant, yet uncertain, driver of Antarctic Ice Sheet mass  
595 loss. (Seroussi et al., 2019, 2020; Cornford et al., 2015; Bulthuis et al., 2019). Of our ocean forcing parameters, the magnitude by which global atmospheric temperature anomalies are scaled to ocean temperature changes  $\alpha$ , appears highly uncertain, amounting to 44% of projection uncertainty in RCP 8.5 (Figure 7). This is consistent with the high sensitivity to the value of  $\alpha$  across the entire Antarctic Ice Sheet (Bulthuis et al., 2019). Going forward, given the impact of a linear scaling and the value of  $\alpha$  on projection uncertainty, it may be more suitable to instead force ocean temperature changes with the results of CMIP ocean  
600 models directly (e.g. the approach used in ISMIP6 proposed by Jourdain et al., 2020). In addition to uncertainties in ocean temperature forcing, it remains challenging to accurately represent ice shelf melt rates, and their sensitivity to temperature changes, in ice-sheet models. While melt parameterisations such as the PICO box model (Reese et al., 2018a) are a substantial advancement in our ability to efficiently apply sub-shelf melting in a physically plausible way, they remain a simplification

---

<sup>c4</sup> uniform

of observed melt rate patterns, and those simulated by ocean models. Hence, it is possible we do not capture the same spatial  
605 distribution or magnitude of melt in highly buttressed regions of the ice shelf as shown in observations, which could ultimately  
impact the (in)stability of the grounding line.

Alongside the mitigating effect of accumulation, using a linear scaling of ocean temperatures, and a simple melt parameterisation, may both be responsible for our simulations not projecting a substantial increase in sub-shelf melt or contribution to global mean sea level rise. Crucially, it appears that we are not capturing the regime shift from 'cold' to 'warm' cavity  
610 conditions as seen in ocean model results (Hellmer et al., 2012; Hazel and Stewart, 2020; Hellmer et al., 2017). Simulations  
by Hellmer et al. (2012) showed relatively warm ocean waters could flush the ice shelf cavity, and increase the area-integrated  
(fixed ice shelf extent) basal mass loss from 80 Gt yr<sup>-1</sup> to 1600 Gt yr<sup>-1</sup> by the year 2100. By comparison, basal mass loss  
during our RCP 8.5 <sup>c1</sup>[training](#) ensemble of simulations (integrated over the initial ice shelf area), reached a maximum of only  
1200 Gt yr<sup>-1</sup> some 200 years later (2300). Beyond our <sup>c2</sup>[training](#) ensemble of 500 simulations, we may start to capture the  
615 same magnitude of basal mass loss, which is reflected in the long-tail of positive contribution to sea level rise in RCP 8.5  
projections. However, the key difference is that melt rates increase at a slow and steady rate over the 150 year period, and do  
not impose a rapid switch from cold to warm conditions which may be possible with a sudden flushing of warm water into the  
ice shelf cavity. <sup>c3</sup>[Additionally, our Bayesian derived probability distributions for ocean forcing parameters, while potentially  
generating more realistic melt rates, may have reduced the probability of sampling high melt rate distributions sufficient to  
620 impose a regime shift that may have occurred with wider sampling.](#) To fully capture such a regime shift, and the effects this  
would have on ice shelf thinning, loss of buttressing, and increases in ice sheet discharge, it is necessary to run fully coupled  
ice–ocean model simulations. Recent work performing coupled simulations on the FR region (Naughten et al., 2021) found  
that ice-shelf melt rates are unlikely to increase over the next century, and thus the region will have a limited contribution to  
sea level rise until ocean temperatures increase substantially (+7°C). While more coupled modelling studies emerge, they are  
625 currently only computationally feasible for regional configurations, and have yet to be accomplished on an ice sheet scale. In  
the meantime, melt parameterisations will remain important for future ice-sheet simulations, and so work should still focus on  
improving their ability to capture the physical behaviour of ocean models, as well as the choice of ocean temperature forcing  
used to perturb those melt rates.

In contrast to atmospheric and oceanic forcing parameters, those related to ice flow dynamics in our model appear to play a  
630 less important role on uncertainties in projections of  $\Delta$ GMSL. Consistent with other studies (Ritz et al., 2015; Bulthuis et al.,  
2019; Gillet-Chaulet et al., 2011; Alevropoulos-Borrill et al., 2020) we have shown that stronger non-linearity in our basal  
sliding and ice flow laws (increasing values of  $m$  and  $n$ ) reduces the response time to a temperature perturbation, allowing  
for faster delivery of ice to the grounding line, and a greater contribution to sea level rise. By varying the value of  $m$  in the  
Weertman sliding law we have captured a large range of amounts of basal sliding, and this has been fully integrated into our  
635 uncertainty analysis. However, this may not have captured the full spread of basal sliding possible under different sliding laws

---

<sup>c1</sup> *Text added.*

<sup>c2</sup> *initial*

<sup>c3</sup> *Text added.*

and/or spatially variable fields of  $m$ . Different sliding laws, (e.g. Budd sliding) may allow for even faster delivery of ice to the grounding line and thus greater contributions to sea level rise (Schlegel et al., 2018; Brondex et al., 2019). We are also not accounting for any transient variability in our basal slipperiness and ice rheology fields, which is not yet captured in most ice flow models, but may additionally increase sea level rise. Progress is being made towards assessing the sensitivity of sea level projections to the choice of sliding law (Brondex et al., 2017, 2019; Cornford et al., 2020). Future work will benefit from choosing the form of the sliding law (Ritz et al., 2015; Gillet-Chaulet et al., 2016), and/or determining spatially variable values for  $m$  (De Rydt et al., 2021; Joughin et al., 2010), that best replicate regional observations of ice loss. This will help to constrain uncertainties associated with the prescription of basal sliding, but this remains an active area of research.

<sup>c1</sup>The surrogate modelling approach used in this study has been a powerful tool for exploring the future behaviour of the FR basin of Antarctica. We have shown that by extensively sampling the parameter space and efficiently propagating this through our surrogate models, we get a greater spread of results, and thus insights into the future of the region, than we would have from our, already large, ensemble . Overall, our <sup>c2</sup>results have shown that regional increases in accumulation assumed with warming are likely to have an important stabilising effect on the ice loss from the FR basin under scenarios of future climate change. There is still some potential for a positive contribution to global mean sea level rise under high sub-shelf melt scenarios. This means that the sign of  $\Delta\text{GMSL}$  projections from the FR basin cannot be fully constrained. Parameters driving both accumulation and sub-shelf melting are highly uncertain and we identify them as priority areas for research, where more accurate parameterisations will help to constrain future projections, not only from the FR basin, but the entire Antarctic Ice Sheet. Future coupled atmospheric–ocean–ice-sheet simulations will help to more accurately capture feed-backs between the atmosphere and ocean on the evolution of the ice-sheet, but remain computationally challenging on a Pan-Antarctic scale. <sup>c3</sup>In addition to coupled simulations, it is important to consider a number of additional processes that have not been captured in our ice flow model simulations. These include: iceberg calving and the retreat of the ice front, evolution of damage of the ice shelf which is becoming of emerging interest in the ice sheet modelling community, and the potential for hydrofracture driven ice shelf collapse under increased surface melt. All of these processes remain highly uncertain, largely due to the challenges of implementation in ice sheet models, but equally have important implications for ice loss and the contribution to global sea level rise, and future work to incorporate these into similar studies is necessary. <sup>c4</sup>Future studies would also benefit from calibrating ice sheet models with observations <sup>c5</sup>in order to reduce uncertainties and constrain future projections by narrowing the parameter space for future simulations based on their fit to observations (Wernecke et al., 2020; Ritz et al., 2015; DeConto and Pollard, 2016; Ritz et al., 2015; Reese et al., 2020). As the number and timespan of observations increases, we will be able to better initialise our ice sheet models to present-day conditions prior to future simulations. Overall, employing uncertainty quantification techniques in future studies will help to provide more robust estimates of potential sea level rise, and identify priority areas for better constraining these projections.

---

<sup>c1</sup> Text added.

<sup>c2</sup> simulations

<sup>c3</sup> Text added.

<sup>c4</sup> In addition to coupled simulations, model calibrations

<sup>c5</sup> can substantially

## 6 Conclusions

This study set out to implement an uncertainty quantification framework (UQLAB) for use alongside the ice flow model Úa and use this to quantify uncertainties in projections of mass loss from the Filchner-Ronne region of Antarctica. We used a novel surrogate modelling approach to extensively sample an input parameter space to determine the forward propagation of uncertainties. Our probabilistic projections indicate that this region may not undergo dramatic ice loss under climate warming scenarios, and instead have a negative contribution to global mean sea level rise. This is primarily due to the effects of increased accumulation assumed with greater moisture content in a warmer climate, that is capable of suppressing mass loss attributed to ocean-driven increases in sub-shelf melt rates. Despite this, we find that there is the potential, albeit highly unlikely, within the bounds of our input parameter space, for a substantial positive contribution to global mean sea level. In these high mass loss scenarios, sub-shelf melting increases enough to outweigh accumulation and force major retreat of some of the ice streams flowing into the FRIS. Uncertainties associated with parameters driving accumulation and sub-shelf melt account for most of the spread of future changes in global mean sea level, and we highlight these as priority areas for constraining projections of ice loss. Future work would benefit from employing uncertainty quantification techniques similar to those used in this study, to fully assess the spread of future projections of sea level rise, not only from the FR basin, but across the entire ice sheet.

## Appendix A: Model inversion for basal slipperiness $C$ and ice rheology $A$ parameters

To estimate the rate factor ( $A$ ) and basal slipperiness coefficient ( $C$ ) for each of our randomly sampled combination of  $m$  and  $n$  we use the inverse capabilities of Úa to minimise the misfit between observed ( $u_{\text{obs}}$ ) and modelled ( $u_{\text{mod}}$ ) velocities. Observed velocities are MEaSUREs InSAR-Based Antarctica ice velocities (Version 2) from 1996 to 2016 and with a spatial resolution  
 685 of 450 m (Rignot et al., 2011; Mouginot et al., 2012). Ice velocities were linearly interpolated onto our model mesh. Úa uses a standard inverse methodology in which a cost function  $J$ , which is the sum of a misfit ( $I$ ) and regularisation ( $R$ ) term, is minimized. The gradients of  $J$  with respect to  $A$  and  $C$  are determined in a computationally efficient way using the adjoint method and Tikhonov-type regularisation. The misfit ( $I$ ) and regularisation ( $R$ ) terms are defined as:

$$I = \frac{1}{2\mathcal{A}} \int (u_{\text{mod}} - u_{\text{obs}})^2 / \epsilon_{\text{obs}}^2 d\mathcal{A} \quad (\text{A1})$$

$$690 \quad R = \frac{1}{2\mathcal{A}} \int (\gamma_s^2 (\nabla \log_{10}(p/\hat{p}))^2 + \gamma_a^2 (\nabla \log_{10}(p/\hat{p}))^2) d\mathcal{A} \quad (\text{A2})$$

where  $\mathcal{A} = \int d\mathcal{A}$  is the area of the model domain,  $\epsilon_{\text{obs}}$  are measurement errors, and  $\hat{p}$  are the a priori values for model parameters ( $\hat{A}$  and  $\hat{C}$ ). Tikhonov regularisation parameters  $\gamma_s$  and  $\gamma_a$  control the slope and amplitude of the gradients in  $A$  and  $C$ . Optimum values were determined using  $L$ -curve analysis and are equal to  $\gamma_s = 10000$  and  $\gamma_a = 1$  for all results presented. The inversions are ran for the number of iterations needed for cost function to converge. The number of iterations needed can vary depending  
 695 on the values of  $m$  and  $n$ . Instead of using a fixed number of iterations, each inversion was terminated when the norm of the function gradient  $|\nabla f(x)|$  becomes sufficiently small. We tested several values for  $|\nabla f(x)|$  and found  $10^{-4}$  was sufficient, and that values any smaller did not substantially improve the cost function, nor substantially affect the transient behaviour in a forward-in-time model run.

Prior to our uncertainty quantification routine (see Section 3.5) we generated a 75 member 'library' of inversions for every  
 700 half integer between 2 and 9 for  $m$  and between 2 and 4 for  $n$ . For these 75 inversions we defined prior values as follows:  $\hat{A} = \epsilon / \tau^n$  with  $\epsilon = 10^{-4} \text{ yr}^{-1}$  and  $\tau_e = 80 \text{ kPa}$  which for  $n = 3$  gives  $\hat{A} \approx 2 \times 10^{-9} \text{ kPa}^{-3} \text{ yr}^{-1}$  equivalent to an ice temperature of approx.  $-25^\circ\text{C}$  using an Arrhenius temperature relation (Cuffey and Paterson, 2010).  $\hat{C} = u_b / \tau_b^m$  with  $u_b = 10 \text{ m yr}^{-1}$  and  $\tau_b = 80 \text{ kPa}$ . This library of inversions was designed to make it computationally feasible to incorporate a model inversion before to every forward model run into our uncertainty analysis. For each of our randomly sampled values of  $m$  and  $n$  we  
 705 select the closest inversion from our library as the a priori values for  $A$  and  $C$ . These priors provide a good initial estimate of the spatial fields of  $A$  and  $C$  which means the subsequent inversions need far less iterations to converge. After each inversion we advected  $C$  beneath the ice shelf to avoid a sharp gradient in  $C$  downstream of the grounding line in the case of glacier advance. We note that the model calculated velocities for each model inversion will vary slightly based on the value of  $m$  and  $n$  used and the resultant fields of  $A$  and  $C$ . However, we find all <sup>c1</sup>training ensemble members ( $N = 500$ ) to provide an optimal

---

<sup>c1</sup> Text added.

710 fit to observations and that the misfit between observed and modelled velocities varies by only  $1 \text{ m yr}^{-1}$ , which is small with respect to measurement errors.

## Appendix B: Bayesian optimisation of ocean box model parameters

The majority of our parameters (Figure 3) are reasonably well constrained, i.e. there is good a priori information on their probably distributions. However, some parameters used to force future simulations of sea level rise from Antarctica are less well known, which could lead to wide and potentially unrealistic estimates of future sea level rise. When prior information on parameter values is poor, it is best to take a non-parametric approach, in which the probability distributions are constructed based on observations. This can be done using Bayes theorem:

$$\pi(\theta|Y) = \ell(\theta; Y)\pi(\theta) \tag{B1}$$

where the posterior probability distribution of  $\theta$  (a hyperparameter) given  $Y$  observations is equal to the likelihood ( $\ell$ ) of  $\theta$  given  $Y$  multiplied by the prior probability distribution  $\pi(\theta)$ . We conduct this analysis on the four 'hyperparameters' used in the box model. These are: the time delay ( $\tau$ ) and scaling coefficient ( $\alpha$ ) used to force changes in ocean temperature through time (Equation 14), and two physical parameters that additionally control sub-shelf melt: the turbulent heat exchange coefficient  $\gamma_T^*$  and the strength of the overturning circulation  $c$  (see Reese et al. (2018a); Olbers and Hellmer (2010)). While some information exists on all these parameters, their bounds and distributions are not well known. The primary aim is not to find single point estimates for these parameters, but obtain an optimal range of parameter values that fit model predicted melt rates to observations. These posterior distributions are then used as input to our uncertainty analysis (see Figure 3). We conduct this Bayesian optimisation using the tools in UQLab, including specifying a prior input model, surrogate models, and the Bayesian inversion itself (Marelli and Sudret, 2014).

### B1 Priors

730 Prior probability distributions of our four parameters take into account any available information on their values before our Bayesian calculation. For the scaling coefficient ( $\alpha$ ) and time delay  $\tau$  we used the values presented in Levermann et al. (2020) (see outline in Section sec:oceanforcing) as the a priori information on the probability distributions of these parameters (Figure B1). While some ranges for the heat exchange coefficient ( $\gamma_T^*$ ) and overturning strength ( $c$ ), have been proposed (Reese et al., 2018a; Olbers and Hellmer, 2010), their probability distributions are unknown. Therefore, we use non-informative priors, i.e. we do not prescribe any prior information about these parameters and use a uniform distribution within the bounds  $c \in [0.1, 9] \text{ Sv m}^3 \text{ kg}^{-1}$  and  $\gamma_T^* \in [5 \times 10^{-6}, 1 \times 10^{-4}] \text{ m s}^{-1}$  given by Reese et al. (2018a); Olbers and Hellmer (2010) (see Figure B1). However, we do know that these parameters are related, and certain combinations mean that the physics in the box model no longer hold Reese et al. (2018a). To specify the dependence between values of  $\gamma_T^*$  and  $c$  and ensure that values outside of these bounds are not sampled, we prescribe a Gaussian copula with a correlation of  $p = 0.9$ . To test the sensitivity

740 of our posterior distributions to our specification of the priors we repeated the analysis for several prior distributions, with or without copulas and found our results were largely insensitive to our priors (Figure B1).

## B2 Surrogate modelling

Rather than use a single area-integrated value of sub-shelf melt, and to preserve some of the spatial distribution of melt rates across the shelf, we chose to tune our parameters to observations, using average melt rates within each melt box. As Bayesian  
 745 analysis requires a large number of iterations to settle on a posterior distribution, we first construct five surrogate models to emulate calculated melt rates in each ocean box. For this we use the same method as our surrogate modelling for changes in global mean sea level (see Section 2). We sample 2000 points from our prior probability distributions using Latin hypercube sampling and use these to directly evaluate sub-shelf melt rates in the box-model. Each simulation is run in a diagnostic mode for our nominal start year of 2000, using observations of topography. We assessed the performance of our surrogate models by  
 750 taking a separate validation sample from the parameter space, and found a good fit between true and surrogate modelled melt rates (Supplementary Figure S10).

## B3 Bayesian inversion

To derive posterior distributions for our hyperparameters in Equation B1 we require three things: 1) prior probability distributions, 2) observations of ice shelf melt rates, and 3) a likelihood function that specifies the likelihood of parameter probability  
 755 distributions given observed and modelled melt rates and associated errors. Prior probability distributions have been outlined above and are shown in Figure B1. Secondly, we take observations of sub-shelf melt rates from Moholdt et al. (2014) and average these within each of our five ocean boxes across the Filchner-Ronne ice shelf (Figure B2). We then assume that average melt rates within each box are independent (uncorrelated) with one another and use a log likelihood function defined in the common format as:

$$760 \quad \ell(\theta, Y) = -\frac{1}{2} \log |\Sigma| - \frac{1}{2} \sum_i \frac{(y_i - f(x_i))^2}{\varepsilon_i^2} \quad (\text{B2})$$

where  $i$  is the box number,  $y$  are observed melt rates,  $f(x)$  are modelled melt rates from the surrogate models, and  $\varepsilon$  is discrepancy term for the melt of each box. Errors associated with model physics are difficult to quantify, so we instead incorporate errors from both measurements  $\sigma_{\text{obs}}^2$  (Moholdt et al., 2014) and the surrogate models  $\sigma_{\text{pce}}^2$ . We then weight this error term ( $w$ ) with the normalised box area with respect to the total ice shelf area.

$$765 \quad \varepsilon_i = w_i \sqrt{\sigma_{\text{obs}}^2(i) + \sigma_{\text{pce}}^2(i)} \quad (\text{B3})$$

We performed a number of sensitivity experiments in which we varied the specification of the discrepancy term in the log likelihood function and found that our posterior distributions are similar, regardless of the choice of discrepancy (see Figure B1).

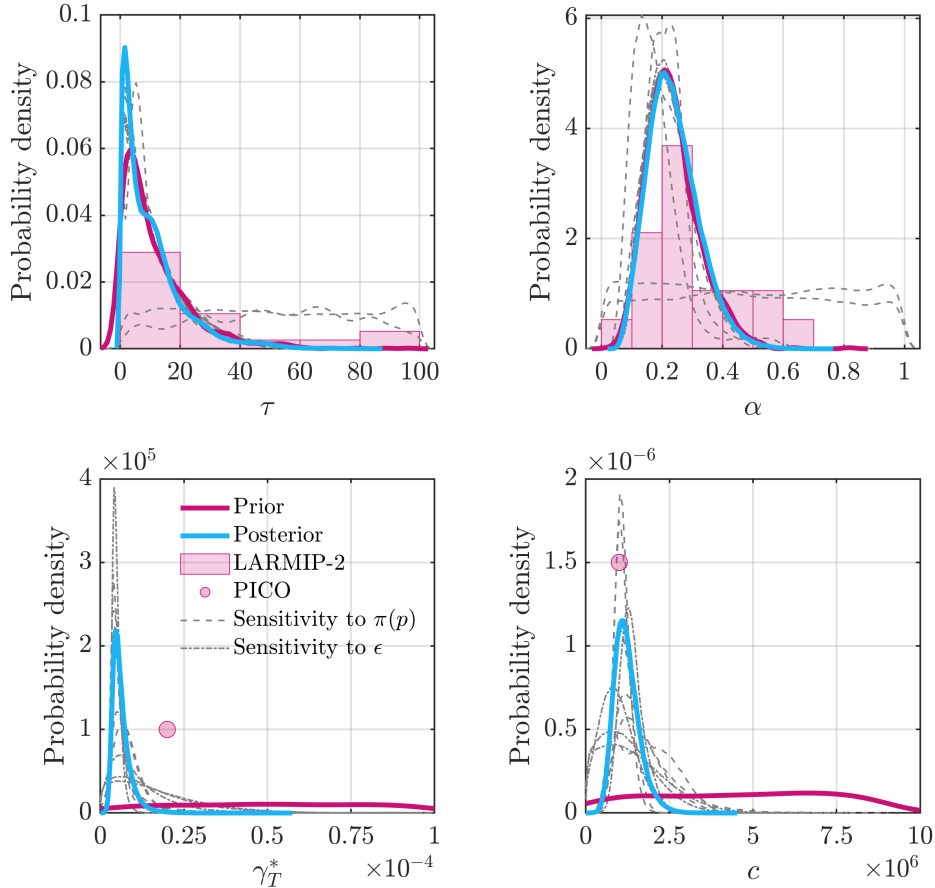


**Figure B1.** Results from our Bayesian analysis. Solid pink line shows priors using uniform bounds for  $\gamma_T^*$  and  $c$  and prior knowledge from the LARMIP-2 distributions for  $\tau$  and  $\alpha$  (pink bars). Solid blue lines show the resultant posterior distributions using the pink lined priors. We performed a number of additional sensitivity experiments in which we varied either the prior distributions (dashed grey line) or the likelihood function (solid grey line). The lines shown are the resultant posterior distributions. These show that our results are largely insensitive to our choice of priors (except in the case of uniform priors for  $\tau$  and  $\alpha$ , which given the information we have are unsuitable) or the likelihood function used. Pink circles show the values proposed for  $\gamma_T^*$  and  $c$  by Reese et al. (2018a) for circum-Antarctic simulations using the PICO box model. Point estimates from our posterior probability distributions show our  $c$  value is close, while values of  $\gamma_T^*$  appear likely to be lower than the value in PICO.

770 Observations for the ocean box closest to the calving front showed high average melt rates ( $0.5 \text{ m yr}^{-1}$ ) which is not related to the overturning circulation in the cavity, but instead seasonal warm surface water intrusions, and will not be replicated by the box model. We therefore choose to replace this with the box average melt from an initial run (using default parameters from Reese et al. (2018a) in Table B1) and reduce the weighting so that it is largely excluded from the analysis. As most ice shelf melt takes place close to the grounding line, far-field melt rates are less important for the total mass balance of the shelf.

775 We specify our priors, likelihood function, and observed melt rates in the Bayesian Inference module in UQLab (Wagner et al., 2019). The posterior probability distributions ( $\pi(\theta|Y)$ ) for our hyperparameters ( $\theta$ ) are then estimated using Monte Carlo Markov Chains (MCMC). We use 1000 independent parallel chains (or sometimes referred to as walkers that move randomly around the parameter space), the starting points of which are randomly sampled initial estimates for  $\theta$  from our prior probability distributions ( $\pi(\theta)$ ). Then an initial step is made from the current position and the posterior probability distribution at that point (which is the product of the likelihood and prior probability see Equation B1) is accepted or rejected using an adaptive metropolis Hastings algorithm (Haario et al., 2001). This is based on whether they are in the right direction from the last sampled point, using an acceptance probability and then the posterior distribution is updated along the way using the information accumulated so far. This process is repeated for 10000 steps for each Markov Chain, by which time the posterior distributions have converged. For more details on MCMC and the adaptive metropolis Hasting algorithm see the UQLab Bayesian Inference Manual (Wagner et al., 2019). We estimate whether the chains have converged on the same <sup>c1</sup>sample point 785 using multivariate potential scale reduction factor (MPSRF: see Brooks and Gelman (1998) and Wagner et al. (2019)), which should approach one if the chains have reached the target posterior distribution. Our final value for MPSRF is 1.01. Finally, it is necessary to post-process the posterior distributions to remove the burn-in steps, which are the steps taken prior to converging on the target posterior distribution. After 2000 steps the posterior distributions have converged (Supplementary Figure S11) so we remove 40% of the posterior sample.

#### 790 **B4 Posterior distributions**

Our posterior probability distributions for all four parameters in the ocean box model are shown in Figure B1 and are input to our uncertainty propagation (Figure 3). These show the distribution of possible values for these parameters that can lead to melt rates closer to observations than non-informative priors. Posterior distributions for  $\tau$  and  $\alpha$  remain close to their priors (Levermann et al., 2020). There is a decreasing likelihood of the delay between increases in atmospheric and ocean 795 temperatures from  $\tau \approx 10$  to 100. The scaling coefficient is centered around 0.24, which is consistent with the scaling factor found to provide a good fit to CMIP5 model data (Taylor et al., 2012; Gollledge et al., 2015). We note that the range for  $\alpha$  is similar to that proposed by Bulthuis et al. (2019) of 0.1 and 0.8, but in this case the posterior distributions are not uniform. In contrast, distributions for  $\gamma_T^*$  and  $c$  have shifted significantly from their prior distributions, and in both cases favour values towards the lower end of prior ranges. Our <sup>c2</sup>parameter point estimate for  $c$  ( $1.2 \text{ Sv m}^3 \text{ kg}^{-1}$ ) is close to the value proposed

---

<sup>c1</sup> Text added.

<sup>c2</sup> Text added.

Point estimates	Prior	Posterior
$\tau$	12	11
$\alpha$	0.23	0.24
$\gamma_T^*$	$2 \times 10^{-5}$	$0.62 \times 10^{-5}$
$c$	$1 \times 10^6$	$1.2 \times 10^6$
$T_o$ (°C)	-1.66	-1.64
BMB (m yr <sup>-1</sup> )	-0.087	-0.133

**Table B1.** Comparison between the forcing temperature and integrated basal mass balance across the total ice shelf for prior and posterior parameter values. In the prior case we use the parameter values for  $\gamma_T^*$  and  $c$  proposed in Reese et al. 2018 and use mean point estimates from our prior distributions for  $\tau$  and  $\alpha$ . Our posterior case uses point estimates for all parameters from our posterior distributions.

800 in Reese et al. (2018a), while  $\gamma_T^*$  is lower but the probability density function still extends to the value in Reese et al. (2018a) (Figure B1).

To examine the performance of our Bayesian inversion, we compare the total area-integrated basal mass balance, i.e. mean specific <sup>c4</sup>basal mass balance, (see Table B1) and spatially averaged melt rates within each box (Figure B2a), for both our prior and posterior <sup>c5</sup>sample point estimates. Using a priori information (values from priors for  $\tau$  and  $\alpha$  and proposed values for <sup>c6</sup> $\gamma_T^*$  and  $c$  from Reese et al. (2018a)) yields an area-integrated basal mass balance (BMB) of  $-0.09$  m yr<sup>-1</sup>. This remains less than half of the BMB from observations  $-0.26$  m yr<sup>-1</sup>. Using the updated <sup>c6</sup>parameter point estimates has brought the BMB closer to observations ( $-0.13$  m yr<sup>-1</sup>), primarily by improving the mean melt rates in boxes 2 and 3 to within the error of observations (Figure B2a). Additionally, we take our model optimised velocities (using an inversion with  $m = 3$  and  $n = 3$ ) and calculate sub-shelf melt rates from ice flux divergence assuming steady-state conditions, i.e. negligible SMB and no surface   
815 thinning/thickening. In this case, BMB is  $-0.15$  m yr<sup>-1</sup>, which suggests that our point parameter estimates are producing near-steady-state melt rates ( $-0.13$  m yr<sup>-1</sup>).

We re-evaluate the surrogate model for the entire prior and posterior sample sets to examine the distribution of melt rates in each ocean box. Figure B2b shows the range of initial melt rates (at start year 2000) close to the grounding line (Box 1) that would have occurred in our uncertainty propagation if we had chosen to use non-informative priors, particularly uniform   
815 distributions for  $\gamma_T^*$  and  $c$ . Given the prior information we have on sub-shelf melt rates (Moholdt et al., 2014), this range of melt rates suggests we would have been sampling unlikely regions of the parameter space. Our Bayesian analysis has successfully tightened the posterior distribution of melt rates, where 5-95% fall within the standard deviation of observations. We can now be confident that our initial <sup>c7</sup> melt rates under the ice shelf at the beginning of our forward simulations is reasonable with respect to observations. We note that our approach estimates these distributions at a single snapshot in time and does not

<sup>c4</sup> surface

<sup>c5</sup> Text added.

<sup>c6</sup> Text added.

<sup>c7</sup> starting point for

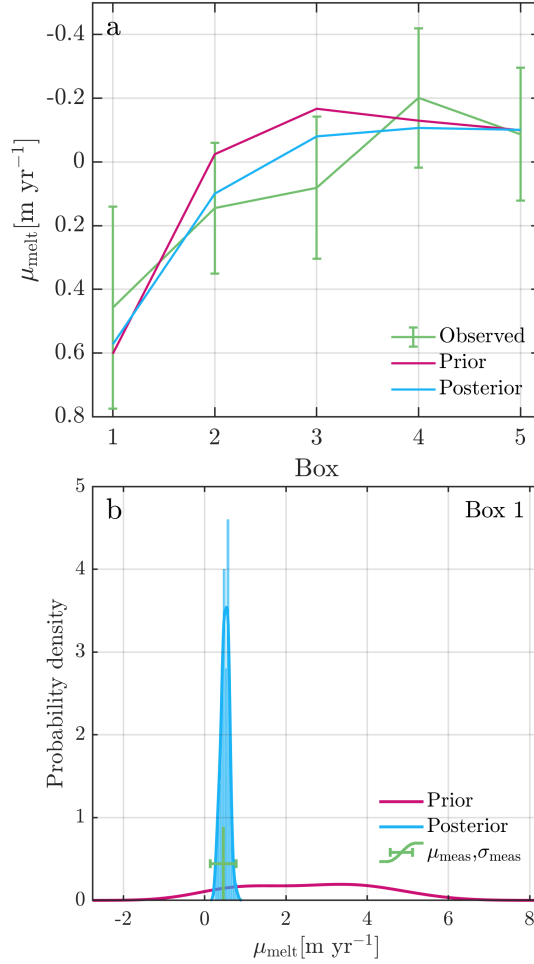


**Figure B2.** a) Observed and modelled mean melt rates ( $\mu_{\text{melt}}$ ) for each box in box-model melt parameterisation. Observations and standard deviations from Moholdt et al. (2014) are shown in green. Pink and blue lines use <sup>c1</sup>sample point estimates from Table B1 to compare prior and posterior box melt rates. Prior melt rates (pink) use the same the parameters for  $\gamma_T^*$  and  $c$  from Reese et al. (2018a) and use mean <sup>c2</sup>sample point estimates from our priors for  $\tau$  and  $\alpha$ . The posterior melt rates (blue) use <sup>c3</sup>sample point estimates from all parameters from our final posterior distributions. b) shows the probability distributions of melt rates in Box 1 (closest to the grounding line) using the entire sample set for both priors and posterior. Note the tight distribution around observations (green) for the posterior sample.

820 take into account variations in these parameters that may occur under future warming e.g. an increase in the strength of the overturning circulation in ice shelf cavities with warmer ocean temperatures.

*Code availability.* The open-source ice flow model *Úa* is available at <https://doi.org/10.5281/zenodo.3706623> (Gudmundsson, 2020) and the ocean box-model for use with *Úa* is available at [https://github.com/shrosier/PICO\\_Ua](https://github.com/shrosier/PICO_Ua). Raw model outputs are available from the authors upon request.

825 *Author contributions.* E.A.H designed and conducted the experiments, and analysed the results. S.H.R.R provided the model set-up for the Filchner-Ronne and the *Úa* implementation of the PICO melt parameterisation. Both S.H.R.R and G.H.G assisted with the the experimental design and model runs. M.C. initially conceived the study and provided input on the uncertainty quantification. E.A.H prepared the manuscript with contributions from all authors.

*Competing interests.* The authors declare that they have no conflict of interest.

830 *Acknowledgements.* This project has received funding from the European Union's Horizon 2020 research and innovation programme under grant agreement no. 820575, and from the NERC grant NE/L013770/1 *Ice shelves in a warming world: Filchner Ice Shelf system, Antarctica*. We acknowledge the use of the Northumbria University HPC facility *Oswald*.

## References

- Alevropoulos-Borrill, A. V., Nias, I. J., Payne, A. J., Golledge, N. R., and Bingham, R. J.: Ocean-forced evolution of the Amundsen Sea catchment, West Antarctica, by 2100, *Cryosphere*, 14, 1245–1258, <https://doi.org/10.5194/tc-14-1245-2020>, 2020.
- Arndt, J. E., Schenke, H. W., Jakobsson, M., Nitsche, F. O., Buys, G., Goleby, B., Rebesco, M., Bohoyo, F., Hong, J., Black, J., Greku, R., Udintsev, G., Barrios, F., Reynoso-Peralta, W., Taisei, M., and Wigley, R.: The International Bathymetric Chart of the Southern Ocean (IBCSO) Version 1.0-A new bathymetric compilation covering circum-Antarctic waters, *Geophysical Research Letters*, 40, 3111–3117, <https://doi.org/10.1002/grl.50413>, 2013.
- Aschwanden, A., Fahnestock, M. A., Truffer, M., Brinkerhoff, D. J., Hock, R., Khroulev, C., Mottram, R., and Abbas Khan, S.: Contribution of the Greenland Ice Sheet to sea level over the next millennium, *Science Advances*, 5, <https://doi.org/10.1126/sciadv.aav9396>, 2019.
- Bengtsson, L., Koumoutsaris, S., and Hodges, K.: Large-Scale Surface Mass Balance of Ice Sheets from a Comprehensive Atmospheric Model, *Surveys in Geophysics*, 32, 459–474, <https://doi.org/10.1007/s10712-011-9120-8>, 2011.
- Blatman, G. and Sudret, B.: Adaptive sparse polynomial chaos expansion based on least angle regression, *Journal of Computational Physics*, 230, 2345–2367, <https://doi.org/10.1016/j.jcp.2010.12.021>, 2011.
- Bons, P. D., Kleiner, T., Llorens, M.-G., Prior, D. J., Sachau, T., Weikusat, I., and Jansen, D.: Greenland Ice Sheet: Higher Nonlinearity of Ice Flow Significantly Reduces Estimated Basal Motion, *Geophysical Research Letters*, 45, 6542–6548, <https://doi.org/10.1029/2018GL078356>, 2018.
- Brondex, J., Gagliardini, O., Gillet-Chaulet, F., and Durand, G.: Sensitivity of grounding line dynamics to the choice of the friction law, *Journal of Glaciology*, 63, 854–866, <https://doi.org/10.1017/jog.2017.51>, 2017.
- Brondex, J., Gillet-Chaulet, F., and Gagliardini, O.: Sensitivity of centennial mass loss projections of the Amundsen basin to the friction law, *The Cryosphere*, 13, 177–195, <https://doi.org/10.5194/tc-13-177-2019>, 2019.
- Brooks, S. P. and Gelman, A.: General Methods for Monitoring Convergence of Iterative Simulations, *Journal of Computational and Graphical Statistics*, 7, 434–455, <https://doi.org/10.1080/10618600.1998.10474787>, 1998.
- Bulthuis, K., Arnst, M., Sun, S., and Pattyn, F.: Uncertainty quantification of the multi-centennial response of the antarctic ice sheet to climate change, vol. 13, <https://doi.org/10.5194/tc-13-1349-2019>, 2019.
- Cornford, S. L., Martin, D. F., Payne, A. J., Ng, E. G., Le Brocq, A. M., Gladstone, R. M., Edwards, T. L., Shannon, S. R., Agosta, C., van den Broeke, M. R., Hellmer, H. H., Krinner, G., Ligtenberg, S. R. M., Timmermann, R., and Vaughan, D. G.: Century-scale simulations of the response of the West Antarctic Ice Sheet to a warming climate, *The Cryosphere*, 9, 1579–1600, <https://doi.org/10.5194/tc-9-1579-2015>, 2015.
- Cornford, S. L., Seroussi, H., Asay-Davis, X. S., Gudmundsson, G. H., Arthern, R., Borstad, C., Christmann, J., Dias dos Santos, T., Feldmann, J., Goldberg, D., Hoffman, M. J., Humbert, A., Kleiner, T., Leguy, G., Lipscomb, W. H., Merino, N., Durand, G., Morlighem, M., Pollard, D., Rückamp, M., Williams, C. R., and Yu, H.: Results of the third Marine Ice Sheet Model Intercomparison Project (MISMIP+), *The Cryosphere*, 14, 2283–2301, <https://doi.org/10.5194/tc-14-2283-2020>, 2020.
- Cuffey, K. M. and Kavanaugh, J. L.: How nonlinear is the creep deformation of polar ice? A new field assessment, *Geology*, 39, 1027–1030, <https://doi.org/10.1130/G32259.1>, 2011.
- Cuffey, K. M. and Paterson, W. S. B.: *The physics of glaciers*, Academic Press, 2010.
- De Rydt, J., Gudmundsson, G. H., Rott, H., and Bamber, J. L.: Modeling the instantaneous response of glaciers after the collapse of the Larsen B Ice Shelf, *Geophysical Research Letters*, 42, 5355–5363, <https://doi.org/10.1002/2015GL064355>, 2015.

- 870 De Rydt, J., Reese, R., Paolo, F. S., and Gudmundsson, G. H.: Drivers of Pine Island Glacier speed-up between 1996 and 2016, *Cryosphere*, 15, 113–132, <https://doi.org/10.5194/tc-15-113-2021>, 2021.
- DeConto, R. M. and Pollard, D.: Contribution of Antarctica to past and future sea-level rise, *Nature*, 531, 591–597, <https://doi.org/10.1038/nature17145>, 2016.
- Edwards, T. L., Brandon, M. A., Durand, G., Edwards, N. R., Golleddge, N. R., Holden, P. B., Nias, I. J., Payne, A. J., Ritz, C., and Wernecke,  
875 A.: Revisiting Antarctic ice loss due to marine ice-cliff instability, *Nature*, 566, 58–64, <https://doi.org/10.1038/s41586-019-0901-4>, 2019.
- Engwirda, D.: Locally optimal Delaunay-refinement and optimisation-based mesh generation, in: Ph.D Thesis, School of Mathematics and Statistics, University of Sydney, <https://ses.library.usyd.edu.au/handle/2123/13148>, 2015.
- Favier, L., Durand, G., Cornford, S. L., Gudmundsson, G. H., Gagliardini, O., Gillet-Chaulet, F., Zwinger, T., Payne, A. J., and  
880 Le Brocq, A. M.: Retreat of Pine Island Glacier controlled by marine ice-sheet instability, *Nature Climate Change*, 4, 117–121, <https://doi.org/10.1038/nclimate2094>, 2014.
- Favier, L., Jourdain, N. C., Jenkins, A., Merino, N., Durand, G., Gagliardini, O., Gillet-Chaulet, F., and Mathiot, P.: Assessment of sub-shelf melting parameterisations using the ocean-ice-sheet coupled model NEMO(v3.6)-Elmer/Ice(v8.3), *Geoscientific Model Development*, 12, 2255–2283, <https://doi.org/10.5194/GMD-12-2255-2019>, 2019.
- Feldmann, J. and Levermann, A.: Collapse of the West Antarctic Ice Sheet after local destabilization of the Amundsen Basin, *Proceedings of  
885 the National Academy of Sciences of the United States of America*, 112, 14 191–14 196, <https://doi.org/10.1073/pnas.1512482112>, 2015.
- Frieler, K., Clark, P. U., He, F., Buizert, C., Reese, R., Ligtenberg, S. R., Van Den Broeke, M. R., Winkelmann, R., and  
Levermann, A.: Consistent evidence of increasing Antarctic accumulation with warming, *Nature Climate Change*, 5, 348–352, <https://doi.org/10.1038/nclimate2574>, 2015.
- Garbe, J., Albrecht, T., Levermann, A., Donges, J. F., and Winkelmann, R.: The hysteresis of the Antarctic Ice Sheet, *Nature*, 585, 538–544,  
890 <https://doi.org/10.1038/s41586-020-2727-5>, 2020.
- Gardner, A. S., Moholdt, G., Scambos, T., Fahnestock, M., Ligtenberg, S., Van Den Broeke, M., and Nilsson, J.: Increased West Antarctic and unchanged East Antarctic ice discharge over the last 7 years, *Cryosphere*, 12, 521–547, <https://doi.org/10.5194/tc-12-521-2018>, 2018.
- Gillet-Chaulet, F., Hindmarsh, R. C., Corr, H. F., King, E. C., and Jenkins, A.: In-situ quantification of ice rheology and direct measurement of the Raymond Effect at Summit, Greenland using a phase-sensitive radar, *Geophysical Research Letters*, 38,  
895 <https://doi.org/10.1029/2011GL049843>, 2011.
- Gillet-Chaulet, F., Durand, G., Gagliardini, O., Mosbeux, C., Mougino, J., Rémy, F., and Ritz, C.: Assimilation of surface velocities acquired between 1996 and 2010 to constrain the form of the basal friction law under Pine Island Glacier, *Geophysical Research Letters*, 43, 311–10, <https://doi.org/10.1002/2016GL069937>, <http://doi.wiley.com/10.1002/2016GL069937>, 2016.
- Glen, J. W.: The creep of polycrystalline ice, *Proceedings of the Royal Society of London. Series A. Mathematical and Physical Sciences*,  
900 228, 519–538, <https://doi.org/10.1098/rspa.1955.0066>, 1955.
- Goelzer, H., Coulon, V., Pattyn, F., de Boer, B., and van de Wal, R.: Brief communication: On calculating the sea-level contribution in marine ice-sheet models, *The Cryosphere*, 14, 833–840, <https://doi.org/10.5194/tc-14-833-2020>, 2020.
- Goldsby, D. L. and Kohlstedt, D. L.: Superplastic deformation of ice: Experimental observations, *Journal of Geophysical Research: Solid Earth*, 106, 11 017–11 030, <https://doi.org/10.1029/2000jb900336>, 2001.
- 905 Golleddge, N. R., Kowalewski, D. E., Naish, T. R., Levy, R. H., Fogwill, C. J., and Gasson, E. G.: The multi-millennial Antarctic commitment to future sea-level rise, *Nature*, 526, 421–425, <https://doi.org/10.1038/nature15706>, 2015.

- Gregory, J. and Huybrechts, P.: Ice-sheet contributions to future sea-level change, *Philosophical Transactions of the Royal Society A: Mathematical, Physical and Engineering Sciences*, 364, 1709–1732, <https://doi.org/10.1098/rsta.2006.1796>, 2006.
- Gudmundsson, G. H.: Ice-shelf buttressing and the stability of marine ice sheets, *The Cryosphere*, 7, 647–655, <https://doi.org/10.5194/tc-7-647-2013>, 2013.
- 910 Gudmundsson, G. H.: GHilmarG/UaSource: Ua2019b (Version v2019b), <https://doi.org/10.5281/zenodo.3706624>, 2020.
- Gudmundsson, G. H. and Jenkins, A.: Ice-flow velocities on Rutford Ice Stream, West Antarctica, are stable over decadal timescales, *Journal of Glaciology*, 55, 339–344, <https://doi.org/10.3189/002214309788608697>, 2009.
- Gudmundsson, G. H., Krug, J., Durand, G., Favier, L., and Gagliardini, O.: The stability of grounding lines on retrograde slopes, *The Cryosphere*, 6, 1497–1505, <https://doi.org/10.5194/tc-6-1497-2012>, 2012.
- 915 Haario, H., Saksman, E., and Tamminen, J.: An adaptive Metropolis algorithm, *Bernoulli*, 7, 223–242, <https://doi.org/10.2307/3318737>, 2001.
- Hazel, J. E. and Stewart, A. L.: Bistability of the Filchner-Ronne Ice Shelf Cavity Circulation and Basal Melt, *Journal of Geophysical Research: Oceans*, 125, <https://doi.org/10.1029/2019JC015848>, 2020.
- 920 Hellmer, H. H., Kauker, F., Timmermann, R., Determann, J., and Rae, J.: Twenty-first-century warming of a large Antarctic ice-shelf cavity by a redirected coastal current, *Nature*, 485, 225–228, <https://doi.org/10.1038/nature11064>, 2012.
- Hellmer, H. H., Kauker, F., Timmermann, R., and Hattermann, T.: The fate of the Southern Weddell sea continental shelf in a warming climate, *Journal of Climate*, 30, 4337–4350, <https://doi.org/10.1175/JCLI-D-16-0420.1>, 2017.
- Hill, E. A., Gudmundsson, G. H., Carr, J. R., and Stokes, C. R.: Velocity response of Petermann Glacier, northwest Greenland, to past and future calving events, *The Cryosphere*, 12, 3907–3921, <https://doi.org/10.5194/tc-12-3907-2018>, 2018.
- 925 IPCC: Climate Change 2014: Synthesis Report. Contribution of Working Groups I, II and III to the Fifth Assessment Report of the Intergovernmental Panel on Climate Change, IPCC, Geneva, Switzerland, 2014.
- Jacka, T. H.: The time and strain required for development of minimum strain rates in ice, *Cold Regions Science and Technology*, 8, 261–268, [https://doi.org/10.1016/0165-232X\(84\)90057-0](https://doi.org/10.1016/0165-232X(84)90057-0), 1984.
- 930 Jacobs, S. S., Jenkins, A., Giulivi, C. F., and Dutrieux, P.: Stronger ocean circulation and increased melting under Pine Island Glacier ice shelf, *Nature Geoscience*, 4, 519–523, <https://doi.org/10.1038/ngeo1188>, 2011.
- Jenkins, A., Dutrieux, P., Jacobs, S. S., McPhail, S. D., Perrett, J. R., Webb, A. T., and White, D.: Observations beneath Pine Island Glacier in West-Antarctica and implications for its retreat, *Nature Geoscience*, 3, 468–472, <https://doi.org/10.1038/ngeo890>, 2010.
- Jezeq, K. C., Alley, R. B., and Thomas, R. H.: Rheology of glacier ice, *Science*, 227, 1335–1338, 1985.
- 935 Joughin, I., Smith, B. E., and Holland, D. M.: Sensitivity of 21st century sea level to ocean-induced thinning of Pine Island Glacier, Antarctica, *Geophysical Research Letters*, 37, <https://doi.org/10.1029/2010GL044819>, 2010.
- Jourdain, N. C., Asay-Davis, X., Hattermann, T., Straneo, F., Seroussi, H., Little, C. M., and Nowicki, S.: A protocol for calculating basal melt rates in the ISMIP6 Antarctic ice sheet projections, *Cryosphere*, 14, 3111–3134, <https://doi.org/10.5194/tc-14-3111-2020>, 2020.
- Kirby, S. H., Durham, W. B., Beeman, M. L., Heard, H. C., and Daley, M. A.: Inelastic properties of ice Ih at low temperatures and high pressures, in: *Journal de Physique (Paris), Colloque*, vol. 48, pp. 227–232, <https://doi.org/10.1051/jphyscol:1987131>, 1987.
- 940 Kittel, C., Amory, C., Agosta, C., Jourdain, N. C., Hofer, S., Delhasse, A., Doutreloup, S., Huot, P. V., Lang, C., Fichet, T., and Fetzweis, X.: Diverging future surface mass balance between the Antarctic ice shelves and grounded ice sheet, *Cryosphere*, 15, 1215–1236, <https://doi.org/10.5194/TC-15-1215-2021>, 2021.

- Krinner, G., Magand, O., Simmonds, I., Genthon, C., and Dufresne, J. L.: Simulated Antarctic precipitation and surface mass balance at the  
945 end of the twentieth and twenty-first centuries, *Climate Dynamics*, 28, 215–230, <https://doi.org/10.1007/s00382-006-0177-x>, 2007.
- Krinner, G., Langeron, C., Ménégoz, M., Agosta, C., and Brutel-Vuilmet, C.: Oceanic forcing of Antarctic climate change: A study using  
a stretched-grid atmospheric general circulation model, *Journal of Climate*, 27, 5786–5800, <https://doi.org/10.1175/JCLI-D-13-00367.1>,  
2014.
- Levermann, A., Winkelmann, R., Nowicki, S., Fastook, J. L., Frieler, K., Greve, R., Hellmer, H. H., Martin, M. A., Meinshausen, M., Mengel,  
950 M., Payne, A. J., Pollard, D., Sato, T., Timmermann, R., Wang, W. L., and Bindshadler, R. A.: Projecting Antarctic ice discharge using  
response functions from SeaRISE ice-sheet models, *Earth System Dynamics*, 5, 271–293, <https://doi.org/10.5194/esd-5-271-2014>, 2014.
- Levermann, A., Winkelmann, R., Albrecht, T., Goelzer, H., Golledge, N. R., Greve, R., Huybrechts, P., Jordan, J., Leguy, G., Martin, D.,  
Morlighem, M., Pattyn, F., Pollard, D., Quiquet, A., Rodehacke, C., Seroussi, H., Sutter, J., Zhang, T., Van Breedam, J., Calov, R., Deconto,  
R., Dumas, C., Garbe, J., Hilmar Gudmundsson, G., Hoffman, M. J., Humbert, A., Kleiner, T., Lipscomb, W. H., Meinshausen, M., Ng, E.,  
955 Nowicki, S. M., Perego, M., Price, S. F., Saito, F., Schlegel, N. J., Sun, S., and Van De Wal, R. S.: Projecting Antarctica’s contribution to  
future sea level rise from basal ice shelf melt using linear response functions of 16 ice sheet models (LARMIP-2), *Earth System Dynamics*,  
11, 35–76, <https://doi.org/10.5194/esd-11-35-2020>, 2020.
- Ligtenberg, S. R., van de Berg, W. J., van den Broeke, M. R., Rae, J. G., and van Meijgaard, E.: Future surface mass balance of the Antarctic  
ice sheet and its influence on sea level change, simulated by a regional atmospheric climate model, *Climate Dynamics*, 41, 867–884,  
960 <https://doi.org/10.1007/s00382-013-1749-1>, 2013.
- MacAyeal, D. R.: Large-scale ice flow over a viscous basal sediment: theory and application to ice stream B, Antarctica, *Journal of Geophys-  
ical Research*, 94, 4071–4087, <https://doi.org/10.1029/jb094ib04p04071>, 1989.
- Marelli, S. and Sudret, B.: UQLab: A Framework for Uncertainty Quantification in Matlab, in: *Vulnerability, Uncertainty, and Risk*, pp.  
2554–2563, American Society of Civil Engineers, Reston, VA, <https://doi.org/10.1061/9780784413609.257>, 2014.
- 965 Marelli, S. and Sudret, B.: UQLab user manual – Polynomial chaos expansions, Tech. rep., Chair of Risk, Safety and Uncertainty Quantifi-  
cation, ETH Zurich, Switzerland, 2019.
- Maris, M. N. A., de Boer, B., Ligtenberg, S. R. M., Crucifix, M., van de Berg, W. J., and Oerlemans, J.: Modelling the evolution of the  
Antarctic ice sheet since the last interglacial, *The Cryosphere*, 8, 1347–1360, <https://doi.org/10.5194/tc-8-1347-2014>, 2014.
- Medley, B. and Thomas, E. R.: Increased snowfall over the Antarctic Ice Sheet mitigated twentieth-century sea-level rise, *Nature Climate  
970 Change*, 9, 34–39, <https://doi.org/10.1038/s41558-018-0356-x>, 2019.
- Meinshausen, M., Meinshausen, N., Hare, W., Raper, S. C., Frieler, K., Knutti, R., Frame, D. J., and Allen, M. R.: Greenhouse-gas emis-  
sion targets for limiting global warming to 2°C, *Nature*, 458, 1158–1162, <https://doi.org/10.1038/nature08017>, [https://www.nature.com/  
articles/nature08017](https://www.nature.com/articles/nature08017), 2009.
- Meinshausen, M., Raper, S. C. B., and Wigley, T. M. L.: Emulating coupled atmosphere-ocean and carbon cycle models with a simpler  
975 model, *MAGICC6-Part 1: Model description and calibration*, *Atmos. Chem. Phys.*, 11, 1417–1456, [https://doi.org/10.5194/acp-11-1417-  
2011](https://doi.org/10.5194/acp-11-1417-2011), 2011.
- Moholdt, G., Padman, L., and Fricker, H. A.: Basal mass budget of Ross and Filchner-Ronne ice shelves, Antarctica, derived from Lagrangian  
analysis of ICESat altimetry, *Journal of Geophysical Research F: Earth Surface*, 119, 2361–2380, <https://doi.org/10.1002/2014JF003171>,  
2014.
- 980 Monaghan, A. J., Bromwich, D. H., and Schneider, D. P.: Twentieth century Antarctic air temperature and snowfall simulations by IPCC  
climate models, *Geophysical Research Letters*, 35, n/a–n/a, <https://doi.org/10.1029/2007GL032630>, 2008.

- Morlighem, M., Rignot, E., Binder, T., Blankenship, D., Drews, R., Eagles, G., Eisen, O., Ferraccioli, F., Forsberg, R., Fretwell, P., Goel, V., Greenbaum, J. S., Gudmundsson, H., Guo, J., Helm, V., Hofstede, C., Howat, I., Humbert, A., Jokat, W., Karlsson, N. B., Lee, W. S., Matsuoka, K., Millan, R., Mouginot, J., Paden, J., Pattyn, F., Roberts, J., Rosier, S., Ruppel, A., Seroussi, H., Smith, E. C., Steinhage, D., Sun, B., Broeke, M. R. d., Ommen, T. D., Wessem, M. v., and Young, D. A.: Deep glacial troughs and stabilizing ridges unveiled beneath the margins of the Antarctic ice sheet, *Nature Geoscience*, 13, 132–137, <https://doi.org/10.1038/s41561-019-0510-8>, 2020.
- 985 Mouginot, J., Scheuchl, B., and Rignot, E.: Mapping of Ice Motion in Antarctica Using Synthetic-Aperture Radar Data, *Remote Sensing*, 4, 2753–2767, <https://doi.org/10.3390/rs4092753>, 2012.
- Mouginot, J., Rignot, E., and Scheuchl, B.: Sustained increase in ice discharge from the Amundsen Sea Embayment, West Antarctica, from 1973 to 2013, *Geophysical Research Letters*, 41, 1576–1584, <https://doi.org/10.1002/2013GL059069>, 2014.
- 990 Nakayama, Y., Manucharyan, G., Zhang, H., Dutrieux, P., Torres, H. S., Klein, P., Seroussi, H., Schodlok, M., Rignot, E., and Menemenlis, D.: Pathways of ocean heat towards Pine Island and Thwaites grounding lines, *Scientific Reports*, 9, 1–9, <https://doi.org/10.1038/s41598-019-53190-6>, 2019.
- Naughten, K. A., De Rydt, J., Rosier, S. H. R., Jenkins, A., Holland, P. R., and Ridley, J. K.: Two-timescale response of a large Antarctic ice shelf to climate change, *Nature Communications*, 12, 1991, <https://doi.org/10.1038/s41467-021-22259-0>, 2021.
- 995 Nias, I. J., Cornford, S. L., Edwards, T. L., Gourmelen, N., and Payne, A. J.: Assessing Uncertainty in the Dynamical Ice Response to Ocean Warming in the Amundsen Sea Embayment, West Antarctica, *Geophysical Research Letters*, <https://doi.org/10.1029/2019GL084941>, 2019.
- Olbers, D. and Hellmer, H.: A box model of circulation and melting in ice shelf caverns, *Ocean Dynamics*, 60, 141–153, <https://doi.org/10.1007/s10236-009-0252-z>, 2010.
- 1000 Palermé, C., Genthon, C., Claud, C., Kay, J. E., Wood, N. B., and L’Ecuyer, T.: Evaluation of current and projected Antarctic precipitation in CMIP5 models, *Climate Dynamics*, 48, 225–239, <https://doi.org/10.1007/s00382-016-3071-1>, 2017.
- Paolo, F. S., Fricker, H. A., and Padman, L.: Volume loss from Antarctic ice shelves is accelerating, *Science*, 348, 327–331, <https://doi.org/10.1126/science.aaa0940>, 2015.
- 1005 Pattyn, F.: Sea-level response to melting of Antarctic ice shelves on multi-centennial timescales with the fast Elementary Thermomechanical Ice Sheet model (f.ETISH v1.0), *Cryosphere*, 11, 1851–1878, <https://doi.org/10.5194/tc-11-1851-2017>, 2017.
- Pattyn, F., Perichon, L., Aschwanden, A., Breuer, B., de Smedt, B., Gagliardini, O., Gudmundsson, G. H., Hindmarsh, R. C. A., Hubbard, A., Johnson, J. V., Kleiner, T., Konovalov, Y., Martin, C., Payne, A. J., Pollard, D., Price, S., Rückamp, M., Saito, F., Souček, O., Sugiyama, S., and Zwinger, T.: Benchmark experiments for higher-order and full-Stokes ice sheet models (ISMIP–HOM), *The Cryosphere*, 2, 95–108, <https://doi.org/10.5194/tc-2-95-2008>, 2008.
- 1010 Pattyn, F., Schoof, C., Perichon, L., Hindmarsh, R. C. A., Bueler, E., de Fleurian, B., Durand, G., Gagliardini, O., Gladstone, R., Goldberg, D., Gudmundsson, G. H., Huybrechts, P., Lee, V., Nick, F. M., Payne, A. J., Pollard, D., Rybak, O., Saito, F., and Vieli, A.: Results of the Marine Ice Sheet Model Intercomparison Project, MISMIIP, *The Cryosphere*, 6, 573–588, <https://doi.org/10.5194/tc-6-573-2012>, 2012.
- Pettit, E. C. and Waddington, E. D.: Ice flow at low deviatoric stress, *Journal of Glaciology*, 49, 359–369, <https://doi.org/10.3189/172756503781830584>, 2003.
- 1015 Pettit, E. C., Waddington, E. D., Harrison, W. D., Thorsteinsson, T., Elsberg, D., Morack, J., and Zumberge, M. A.: The crossover stress, anisotropy and the ice flow law at Siple Dome, West Antarctica, *Tech. Rep. 201*, <https://doi.org/10.3189/002214311795306619>, 2011.

- Pollard, D., Chang, W., Haran, M., Applegate, P., and DeConto, R.: Large ensemble modeling of the last deglacial retreat of the West Antarctic Ice Sheet: Comparison of simple and advanced statistical techniques, *Geoscientific Model Development*, 9, 1697–1723, <https://doi.org/10.5194/gmd-9-1697-2016>, 2016.
- 1020 Pritchard, H. D., Ligtenberg, S. R., Fricker, H. A., Vaughan, D. G., Van Den Broeke, M. R., and Padman, L.: Antarctic ice-sheet loss driven by basal melting of ice shelves, *Nature*, 484, 502–505, <https://doi.org/10.1038/nature10968>, 2012.
- Reese, R., Albrecht, T., Mengel, M., Asay-Davis, X., Winkelmann, R., and Sea, A.: Antarctic sub-shelf melt rates via PICO, *Cryosphere*, 12, 1969–1985, <https://doi.org/10.5194/tc-12-1969-2018>, 2018a.
- 1025 Reese, R., Winkelmann, R., and Gudmundsson, G. H.: Grounding-line flux formula applied as a flux condition in numerical simulations fails for buttressed Antarctic ice streams, *The Cryosphere*, 12, 3229–3242, <https://doi.org/10.5194/tc-12-3229-2018>, 2018b.
- Reese, R., Levermann, A., Albrecht, T., Seroussi, H., and Winkelmann, R.: The role of history and strength of the oceanic forcing in sea level projections from Antarctica with the Parallel Ice Sheet Model, *The Cryosphere*, 14, 3097–3110, <https://doi.org/10.5194/tc-14-3097-2020>, 2020.
- 1030 Rignot, E., Mouginot, J., and Scheuchl, B.: Ice flow of the Antarctic Ice Sheet, *Science*, 333, 1427–1430, <https://doi.org/10.1126/science.1208336>, 2011.
- Rignot, E., Mouginot, J., Morlighem, M., Seroussi, H., and Scheuchl, B.: Widespread, rapid grounding line retreat of Pine Island, Thwaites, Smith, and Kohler glaciers, West Antarctica, from 1992 to 2011, *Geophysical Research Letters*, 41, 3502–3509, <https://doi.org/10.1002/2014GL060140>, 2014.
- 1035 Rignot, E., Mouginot, J., Scheuchl, B., Van Den Broeke, M., Van Wessem, M. J., and Morlighem, M.: Four decades of Antarctic Ice Sheet mass balance from 1979–2017, <https://doi.org/10.1073/pnas.1812883116>, 2019.
- Ritz, C., Edwards, T. L., Durand, G., Payne, A. J., Peyaud, V., and Hindmarsh, R. C.: Potential sea-level rise from Antarctic ice-sheet instability constrained by observations, *Nature*, 528, 115–118, <https://doi.org/10.1038/nature16147>, 2015.
- Rodehacke, C. B., Pfeiffer, M., Semmler, T., Gurses, Ö., and Kleiner, T.: Future sea level contribution from Antarctica inferred from CMIP5 model forcing and its dependence on precipitation ansatz, *Earth System Dynamics*, 11, 1153–1194, <https://doi.org/10.5194/esd-11-1153-2020>, 2020.
- 1040 Rosier, S. H., Hofstede, C., Brisbourne, A. M., Hattermann, T., Nicholls, K. W., Davis, P. E., Anker, P. G., Hillenbrand, C. D., Smith, A. M., and Corr, H. F.: A New Bathymetry for the Southeastern Filchner-Ronne Ice Shelf: Implications for Modern Oceanographic Processes and Glacial History, *Journal of Geophysical Research: Oceans*, 123, 4610–4623, <https://doi.org/10.1029/2018JC013982>, 2018.
- 1045 Ross, N., Bingham, R. G., Corr, H. F., Ferraccioli, F., Jordan, T. A., Le Brocq, A., Rippin, D. M., Young, D., Blankenship, D. D., and Siegert, M. J.: Steep reverse bed slope at the grounding line of the Weddell Sea sector in West Antarctica, *Nature Geoscience*, 5, 393–396, <https://doi.org/10.1038/ngeo1468>, 2012.
- Schlegel, N. J., Larour, E., Seroussi, H., Morlighem, M., and Box, J. E.: Ice discharge uncertainties in Northeast Greenland from boundary conditions and climate forcing of an ice flow model, *Journal of Geophysical Research: Earth Surface*, 120, 29–54, <https://doi.org/10.1002/2014JF003359>, 2015.
- 1050 Schlegel, N. J., Seroussi, H., Schodlok, M. P., Larour, E. Y., Boening, C., Limonadi, D., Watkins, M. M., Morlighem, M., and Van Den Broeke, M. R.: Exploration of Antarctic Ice Sheet 100-year contribution to sea level rise and associated model uncertainties using the ISSM framework, *Cryosphere*, 12, 3511–3534, <https://doi.org/10.5194/tc-12-3511-2018>, 2018.
- Schmidtko, S., Heywood, K. J., Thompson, A. F., and Aoki, S.: Multidecadal warming of Antarctic waters, *Science*, 346, 1227–1231, <https://doi.org/10.1126/science.1256117>, 2014.
- 1055

- Seroussi, H. and Morlighem, M.: Representation of basal melting at the grounding line in ice flow models, *The Cryosphere*, 12, 3085–3096, <https://doi.org/10.5194/tc-12-3085-2018>, 2018.
- 1060 Seroussi, H., Nowicki, S., Simon, E., Abe-Ouchi, A., Albrecht, T., Brondex, J., Cornford, S., Dumas, C., Gillet-Chaulet, F., Goelzer, H., Gолledge, N. R., Gregory, J. M., Greve, R., Hoffman, M. J., Humbert, A., Huybrechts, P., Kleiner, T., Larour, E., Leguy, G., Lipscomb, W. H., Lowry, D., Mengel, M., Morlighem, M., Pattyn, F., Payne, A. J., Pollard, D., Price, S. F., Quiquet, A., Reerink, T. J., Reese, R., Rodehacke, C. B., Schlegel, N. J., Shepherd, A., Sun, S., Sutter, J., Van Breedam, J., Van De Wal, R. S., Winkelmann, R., and Zhang, T.: InitMIP-Antarctica: An ice sheet model initialization experiment of ISMIP6, *Cryosphere*, 13, 1441–1471, <https://doi.org/10.5194/tc-13-1441-2019>, 2019.
- 1065 Seroussi, H., Nowicki, S., Payne, A. J., Goelzer, H., Lipscomb, W. H., Abe-Ouchi, A., Agosta, C., Albrecht, T., Asay-Davis, X., Barthel, A., Calov, R., Cullather, R., Dumas, C., Galton-Fenzi, B. K., Gladstone, R., Gолledge, N. R., Gregory, J. M., Greve, R., Hattermann, T., Hoffman, M. J., Humbert, A., Huybrechts, P., Jourdain, N. C., Kleiner, T., Larour, E., Leguy, G. R., Lowry, D. P., Little, C. M., Morlighem, M., Pattyn, F., Pelle, T., Price, S. F., Quiquet, A., Reese, R., Schlegel, N. J., Shepherd, A., Simon, E., Smith, R. S., Straneo, F., Sun, S., Trusel, L. D., Breedam, J. V., Van De Wal, R. S., Winkelmann, R., Zhao, C., Zhang, T., and Zwinger, T.: ISMIP6 Antarctica: A multi-model ensemble of the Antarctic ice sheet evolution over the 21st century, <https://doi.org/10.5194/tc-14-3033-2020>, 2020.
- 1070 Shepherd, A., Ivins, E., Rignot, E., Smith, B., Van Den Broeke, M., Velicogna, I., Whitehouse, P., Briggs, K., Joughin, I., Krinner, G., Nowicki, S., Payne, T., Scambos, T., Schlegel, N., Geruo, A., Agosta, C., Ahlstrøm, A., Babonis, G., Barletta, V., Blazquez, A., Bonin, J., Csatho, B., Cullather, R., Felikson, D., Fettweis, X., Forsberg, R., Gallee, H., Gardner, A., Gilbert, L., Groh, A., Gunter, B., Hanna, E., Harig, C., Helm, V., Horvath, A., Horwath, M., Khan, S., Kjeldsen, K. K., Konrad, H., Langen, P., Lecavalier, B., Loomis, B., Luthcke, S., McMillan, M., Melini, D., Mernild, S., Mohajerani, Y., Moore, P., Mouginit, J., Moyano, G., Muir, A., Nagler, T., Nield, G., Nilsson, J., 1075 Noel, B., Ootaka, I., Pattle, M. E., Peltier, W. R., Pie, N., Rietbroek, R., Rott, H., Sandberg-Sørensen, L., Sasgen, I., Save, H., Scheuchl, B., Schrama, E., Schröder, L., Seo, K. W., Simonsen, S., Slater, T., Spada, G., Sutterley, T., Talpe, M., Tarasov, L., Van De Berg, W. J., Van Der Wal, W., Van Wessel, M., Vishwakarma, B. D., Wiese, D., and Wouters, B.: Mass balance of the Antarctic Ice Sheet from 1992 to 2017, <https://doi.org/10.1038/s41586-018-0179-y>, 2018.
- 1080 Shepherd, A., Gilbert, L., Muir, A. S., Konrad, H., McMillan, M., Slater, T., Briggs, K. H., Sundal, A. V., Hogg, A. E., and Engdahl, M. E.: Trends in Antarctic Ice Sheet Elevation and Mass, *Geophysical Research Letters*, 46, 8174–8183, <https://doi.org/10.1029/2019GL082182>, 2019.
- Sudret, B.: Uncertainty propagation and sensitivity analysis in mechanical models—Contributions to structural reliability and stochastic spectral methods, *Habilitationa diriger des recherches*, Université Blaise Pascal, Clermont-Ferrand, France, 147, 2007.
- 1085 Tang, M. S., Chenoli, S. N., Samah, A. A., and Hai, O. S.: An assessment of historical Antarctic precipitation and temperature trend using CMIP5 models and reanalysis datasets, *Polar Science*, 15, 1–12, <https://doi.org/10.1016/j.polar.2018.01.001>, 2018.
- Taylor, K. E., Stouffer, R. J., and Meehl, G. A.: An overview of CMIP5 and the experiment design, <https://doi.org/10.1175/BAMS-D-11-00094.1>, 2012.
- Thoma, M., Jenkins, A., Holland, D., and Jacobs, S.: Modelling Circumpolar Deep Water intrusions on the Amundsen Sea continental shelf, Antarctica, *Geophysical Research Letters*, 35, L18 602, <https://doi.org/10.1029/2008GL034939>, 2008.
- 1090 Thomas, R. H.: The Creep of Ice Shelves: Theory, *Journal of Glaciology*, 12, 45–53, <https://doi.org/10.3189/s002214300002270x>, 1973.
- Treverrow, A., Budd, W. F., Jacka, T. H., and Warner, R. C.: The tertiary creep of polycrystalline ice: Experimental evidence for stress-dependent levels of strain-rate enhancement, *Journal of Glaciology*, 58, 301–314, <https://doi.org/10.3189/2012JoG11J149>, 2012.

- 1095 Van Wessem, J. M., Reijmer, C. H., Morlighem, M., Mouginot, J., Rignot, E., Medley, B., Joughin, I., Wouters, B., Depoorter, M. A., Bamber, J. L., Lenaerts, J. T., Van De Berg, W. J., Van Den Broeke, M. R., and Van Meijgaard, E.: Improved representation of East Antarctic surface mass balance in a regional atmospheric climate model, *Journal of Glaciology*, 60, 761–770, <https://doi.org/10.3189/2014JG14J051>, 2014.
- Wagner, P.-R., Nagel, J., Marelli, S., and Sudret, B.: UQLab user manual – Bayesian inversion for model calibration and validation, Tech. rep., Chair of Risk, Safety and Uncertainty Quantification, ETH Zurich, Switzerland, 2019.
- 1100 Wernecke, A., Edwards, T. L., Nias, I. J., Holden, P. B., and Edwards, N. R.: Spatial probabilistic calibration of a high-resolution Amundsen Sea Embayment ice sheet model with satellite altimeter data, *The Cryosphere*, 14, 1459–1474, <https://doi.org/10.5194/tc-14-1459-2020>, 2020.
- Winkelmann, R., Levermann, A., Martin, M. A., and Frieler, K.: Increased future ice discharge from Antarctica owing to higher snowfall, *Nature*, 492, 239–242, <https://doi.org/10.1038/nature11616>, 2012.
- 1105 Wright, A. P., Le Brocq, A. M., Cornford, S. L., Bingham, R. G., Corr, H. F., Ferraccioli, F., Jordan, T. A., Payne, A. J., Rippin, D. M., Ross, N., and Siegert, M. J.: Sensitivity of the Weddell Sea sector ice streams to sub-shelf melting and surface accumulation, *Cryosphere*, 8, 2119–2134, <https://doi.org/10.5194/tc-8-2119-2014>, 2014.